Check for updates

Received: 26 August 2024 | Revised: 13 November 2024 | Accepted: 28 December 2024

DOI: 10.1002/qj.4936

Quarterly Journal of the Royal Meteorological Society RMetS

RESEARCH ARTICLE

Heavy summer rainfall in southeastern Australia

Cameron R. Henderson[1,2] | **Michael A. Barnes**[2,3] | **Michael J. Reeder**[2,3] | **Julian F. Quinting**[2,3,4] | **Christian Jakob**[2,3,5]

[1]Bureau of Meteorology Training Centre, Broadmeadows, Victoria Australia

[2]School of Earth, Atmosphere and Environment, Monash University, Clayton, Victoria Australia

[3]Australian Research Council Centre of Excellence for Climate Extremes, Monash University, Clayton, Victoria Australia

[4]Institute of Meteorology and Climate Research Troposphere Research (IMK-TRO), Karlsruhe Institute of Technology, Karlsruhe, Germany

[5]Australian Research Council Centre of Excellence for the Weather of the 21st Century, Monash University, Clayton, Victoria Australia

Correspondence
Cameron R. Henderson, School of Earth, Atmosphere and Environment, Monash University, Building 28, 9 Rainforest Walk, Clayton Campus, Clayton, VIC 3800, Australia.
Email: cameron.henderson@monash.edu

Funding information
Australian Research Council, Grant/Award Numbers: CE170100023, CE230100012; Helmholtz Association, Grant/Award Number: VH-NG-1243

Abstract

In the austral summer, parts of southeastern Australia are prone to heavy rainfall that causes major riverine flooding and fatalities. Easterly flow associated with an anticyclone in the Tasman Sea, large moisture transports from the Coral Sea, and upper tropospheric cyclonic disturbances all contribute to these heavy rainfall episodes. However, questions regarding their synoptic dynamics remain, including which of these ingredients are the most critical. These questions are addressed by comparing composite pressure and moisture fields of heavy rainfall days over selected regions with non-heavy rainfall days that have a similar synoptic pattern. A synoptic climatology is constructed for this purpose by *k*-means cluster analysis of 500 hPa geopotential height anomalies from the European Centre for Medium-range Weather Forecasts Reanalysis v5, for all December to March days over a period of 40 years. Heavy rainfall days in the wettest clusters have negative 500 hPa geopotential height anomalies immediately west of the affected region that are stronger on average than those of non-heavy rainfall days. Their accompanying distributions of surface pressure, precipitable water, and vertical motion are consistent with cyclonic baroclinic development and are preceded by anticyclonic Rossby wave breaking. Heavy rainfall days also show an increased frequency of blocking near 150° E; however, this peaks 1–2 days *after* the onset of heavy rain. Regional rainfall in these clusters shows strong sensitivity to lower pressure immediately westward but little sensitivity to high pressure in the Tasman Sea until after the commencement of rain. A companion study using the same cluster analysis illustrated the link between anticyclonic Rossby wave breaking and heatwaves in southeastern Australia. These latest results highlight the upper cyclonic anomalies that often form on the equatorward flank of anticyclonic Rossby wave breaking as the key ingredient separating days with a favourable synoptic-scale pattern of surface high pressure into those that rain heavily and those that do not.

KEYWORDS

cluster analysis, Rossby wave breaking, southeastern Australia

This is an open access article under the terms of the Creative Commons Attribution-NonCommercial License, which permits use, distribution and reproduction in any medium, provided the original work is properly cited and is not used for commercial purposes.
© 2025 The Author(s). *Quarterly Journal of the Royal Meteorological Society* published by John Wiley & Sons Ltd on behalf of Royal Meteorological Society.

1 | INTRODUCTION

Written records of heavy rainfall in southeastern Australia stretch back more than 150 years, with detailed accounts of major riverine flooding and numerous fatalities (Callaghan & Power, 2014). Occurring with greater frequency over the warmer months (Warren *et al.*, 2021; White *et al.*, 2022), heavy rainfall has affected many parts of southeastern Australia (Figure 1) in the December–March (DJFM) period (Bureau of Meteorology, 2012, 2013, 2016, 2021, 2022). Eastern coastal regions are especially affected, with most of these recent extreme events delivering near or in excess of 400 mm to lengthy stretches of coastline. In the February to March 2022 event, more than 1,000 mm fell at several rain-gauges in southeastern Queensland and northeastern New South Wales (NSW), with record flooding in some river catchments. Other than the January 2013 event that mainly affected southeastern Queensland, these rainfall events did not result from ex-tropical cyclones. Thus, determining how weather systems interact with tropical moisture reservoirs to produce heavy rainfall is important for understanding these natural disasters.

Most of southeastern Australia lies in the Subtropics of the Southern Hemisphere. For the purpose of this study it is defined as Australian land areas south of 27° S and east of 138° E, including Tasmania (all land areas within the black border in Figure 2). This is the most densely inhabited region of the country and includes the most populous state capital cities of Sydney, Melbourne, and Brisbane. There is a gradual transition, from greater tropical influence with increased rainfall during the warm season in the north, to midlatitude weather and rainfall that is more evenly distributed across the seasons in the south (Bureau of Meteorology, 2024; Speer *et al.*, 2011).

Composite mean-sea-level pressure (MSLP) patterns of heavy rainfall along the eastern seaboard[1] show a surface anticyclone in the southeastern Tasman Sea, a surface pressure trough offshore and adjacent to the coast, and an associated east to northeasterly flow over the western Tasman Sea and southeastern Australia (Barnes *et al.*, 2023; Black & Lane, 2015). Easterly flows, especially when coupled with midtropospheric ascent, have a strong correlation with eastern seaboard rainfall over seasonal time-scales (Black & Lane, 2015), although the relationship is weaker over daily time-scales. Much of the moisture that is precipitated over southeastern Australia in the austral summer originates from the Coral Sea and northwestern Tasman Sea (Gimeno *et al.*, 2010; Holgate *et al.*, 2020), and heavy rainfall on the eastern seaboard is typically associated with large vertically integrated horizontal transports of water vapour from this region (Barnes *et al.*, 2023; Reid *et al.*, 2021; Warren *et al.*, 2021; White *et al.*, 2022).

More than 20% of heavy rainfall in DJFM along the eastern seaboard, and neighbouring coastal regions, extending southwest to the most southern point of Victoria, is attributable to east coast lows (Pepler *et al.*, 2014, their fig. 4), a fraction that increases to above 50% during winter. For these systems it is also found that the rainfall is heavier and more widespread when a cyclonic circulation is also observed at 500 hPa over southeastern Australia (Pepler & Dowdy, 2021).

Several other studies have demonstrated that a nearby upper level trough or cut-off cyclonic vortex is a key ingredient of heavy rainfall over southeastern Australia (Barnes *et al.*, 2023; Pook *et al.*, 2006; Pook *et al.*, 2013; Risbey *et al.*, 2009a; Warren *et al.*, 2021). In their rain-gauge-based comparison of heavy and extreme rainfall for the cities of Brisbane, Sydney, and Melbourne, Warren *et al.* (2021).[2] found that extreme rainfall has a more amplified trough or cut-off low at 500 hPa. Barnes *et al.* (2023) found that slow-moving cut-off upper level cyclonic vortices, and their associated region of downstream ascent, are particularly effective at producing heavy rainfall. The higher frequency of slow-moving cut-off upper level cyclones over the warmer months (their Figure 4) can also explain the higher frequency of eastern seaboard heavy rainfall at this time of year reported by Warren *et al.* (2021) and White *et al.* (2022).

Atmospheric blocking, associated with increased rainfall over southeastern Australia (Risbey *et al.*, 2009b), refers to the formation of slow-moving anticyclones at high latitudes, often termed blocking highs. It is also characterised by a split jet in the mid-upper troposphere and, frequently, a cut-off cyclone on the equatorward, westward flank of the upper ridge (Coughlan, 1983; Pelly & Hoskins, 2003). This configuration arises as a result of anticyclonic Rossby wave breaking (Barnes *et al.*, 2021; Berrisford *et al.*, 2007; Ndarana & Waugh, 2011; Thorncroft *et al.*, 1993), which is common at southeast Australian longitudes during the austral summer (Reeder *et al.*, 2015) and is also closely linked to heatwaves in Victoria (Henderson *et al.*, 2024; Parker *et al.*, 2013, 2014; Quinting & Reeder, 2017). Cyclonic Rossby wave breaking can also lead to blocking (Masato *et al.*, 2012) but is much less common than anticyclonic Rossby wave breaking at the latitudes of mainland Australia at this time of year (Song *et al.*, 2011, fig. 4). Strong and widespread correlations have been found between blocking near 120°E to 150°E and rainfall over southeastern Australia during winter and spring (Pook *et al.*, 2013; Risbey *et al.*, 2009b), although the relationship is much weaker during summer. This is somewhat surprising, as blocking that results in enhanced precipitation is usually associated with cut-off lows (Pook *et al.*, 2013), which make a major contribution to heavy

1477870x, 0, Downloaded from https://rmets.onlinelibrary.wiley.com/doi/10.1002/qj.4936 by Karlsruher Institut Für Technologie, Wiley Online Library on [31/03/2025]. See the Terms and Conditions (https://onlinelibrary.wiley.com/terms-and-conditions) on Wiley Online Library for rules of use; OA articles are governed by the applicable Creative Commons License

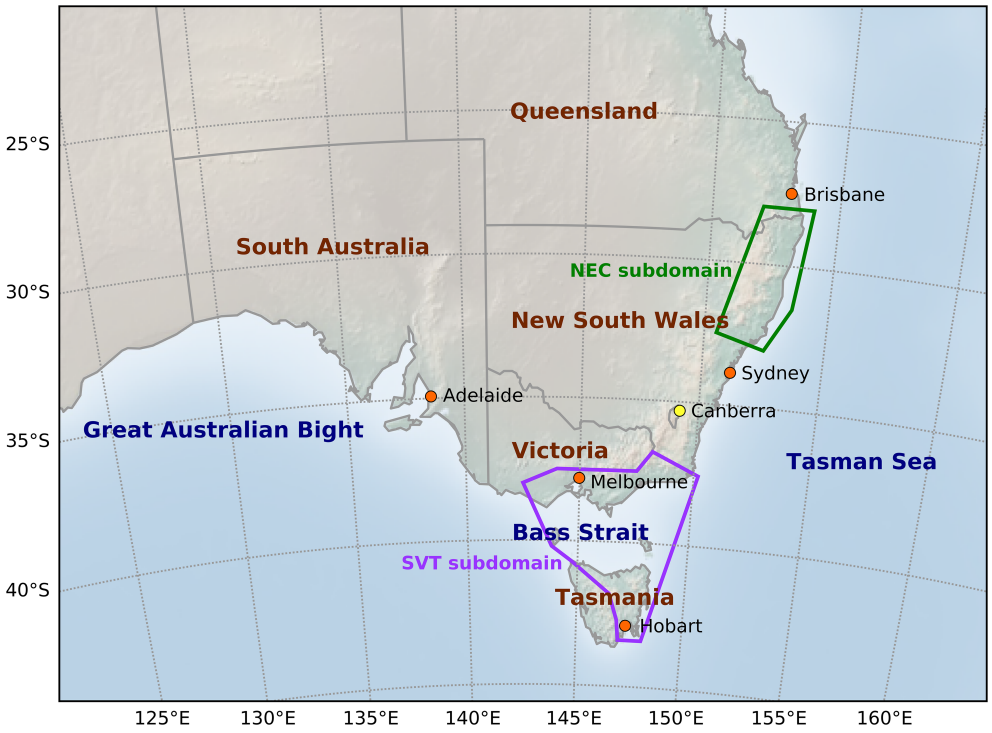

FIGURE 1 States and capital cities of southeastern Australia, and surrounding seas. The Great Dividing Range adjacent to Australia's east coast is visible in the topographic relief. Coloured polygons correspond to the northern coast of eastern New South Wales (NEC) subdomain (green) and the southern Victoria and eastern Tasmania (SVT) subdomain (purple). [Colour figure can be viewed at wileyonlinelibrary.com]

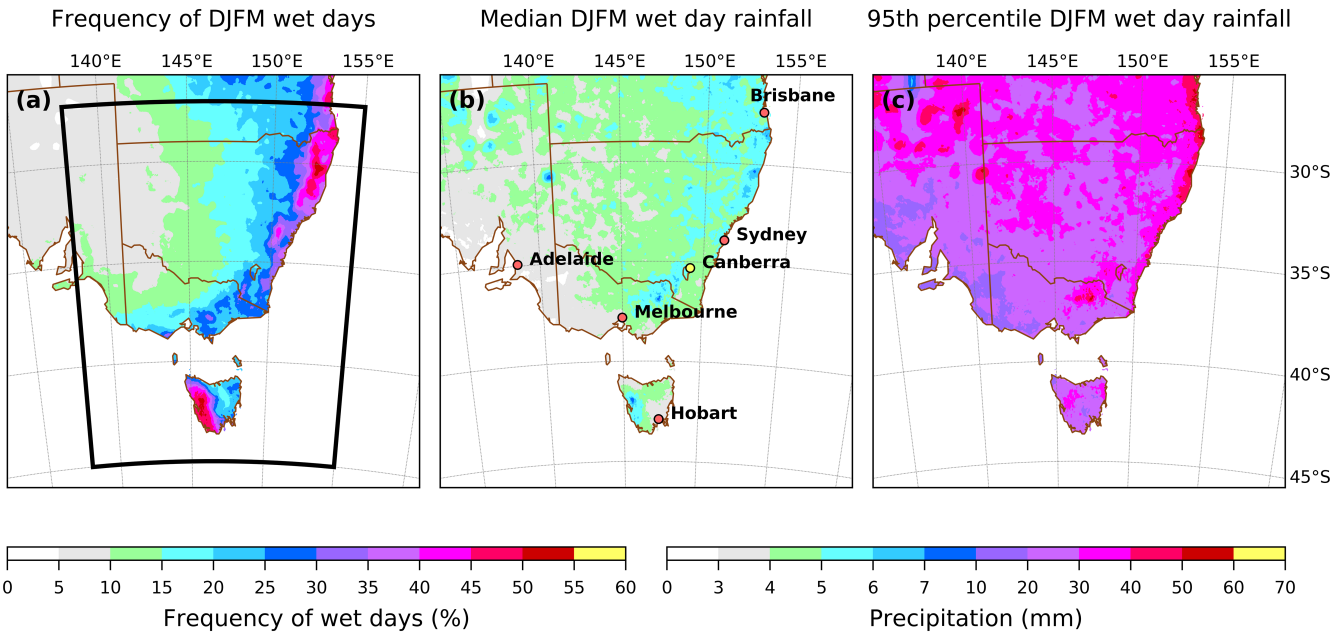

FIGURE 2 (a) Frequency of December–March (DJFM) wet days with rainfall ≥1 mm over southeastern Australia (black border), (b) median wet-day rainfall, and (c) the 95th percentile of wet-day rainfall at each grid point across southeastern Australia. The same scale is used in (b) and (c). State capital cities are shown with red dots and labels in (b), and the national capital Canberra is marked with a yellow dot. [Colour figure can be viewed at wileyonlinelibrary.com]

summer rainfall over southeastern Australia (Barnes *et al.*, 2023).

The aforementioned studies have identified several important ingredients of heavy rainfall over southeastern Australia: (a) an anticyclone in the Tasman Sea that is often slow moving enough to be considered blocking, (b) an easterly flow across the Great Dividing Range, (c) a surface trough or east coast low, (d) enhanced moisture, and (e) an upper level trough or cut-off low. Uncertainty still exists over their relative importance and the extent

1477870x, 0, Downloaded from https://rmets.onlinelibrary.wiley.com/doi/10.1002/qj.4936 by Karlsruher Institut Für Technologie, Wiley Online Library on [31/03/2025]. See the Terms and Conditions (https://onlinelibrary.wiley.com/terms-and-conditions) on Wiley Online Library for rules of use; OA articles are governed by the applicable Creative Commons License

to which one ingredient causes the others. For instance, a surface anticyclone in the south Tasman Sea results in geostrophic easterly flow over southeastern Australia. Moreover, a strong ascending component to the east coast flow index (Black & Lane, 2015) can often be explained by the presence of an upper level cut-off cyclone over southeastern Australia (Barnes *et al.*, 2023). In a global study, de Vries (2021, fig. 13). reported that extreme rainfall in southeastern Australia could be linked to the combined influence of Rossby wave breaking and organised structures of large vertically integrated horizontal water vapour transport more than 50% of the time.

In the present DJFM study, the relative importance of these ingredients of heavy rainfall days are assessed by comparison with all other days on which a similar synoptic-scale weather pattern occurred (and did not produce heavy rainfall). A seven-state synoptic climatology is constructed by *k*-means cluster analysis for this purpose, and a subset of the clusters that are notably associated with wet weather over southeastern Australia are analysed in detail. Subdomains that receive the highest rainfall in these clusters are identified, and composite fields of pressure and moisture on their heavy rain days are compared with those of all other days. Midlatitude Rossby wave propagation and blocking in both categories are juxtaposed in Hovmöller diagrams showing potential vorticity (PV) at either 330 K or 350 K, anticyclonic Rossby wave breaking frequency, and Tibaldi–Molteni blocking index (TMBI). Finally, the ensemble sensitivity technique (Torn & Hakim, 2008) is applied to normalised rainfall anomalies in these subdomains to measure the strength of correlations with pressure and moisture fields in the corresponding cluster.

The datasets and methods used in this article are explained in Section 2, and the composite pressure and rainfall patterns of the synoptic climatology are presented in Section 3. The comparison of heavy rainfall days with non-heavy rainfall days for selected clusters and subdomains is presented in Section 4. This is followed by the sensitivity analysis in Section 5, with conclusions in Section 6.

2 | DATA AND METHOD

2.1 | Data

Gridded rainfall data at 0.05° × 0.05° horizontal resolution from the Australian Water Availability Project (AWAP) Jones *et al.* (2009) are used to define wet days and heavy rainfall days over Australian land. These are available as rainfall accumulations over the previous 24 hr to 0900 h local time. All other parameters consist of instantaneous fields sampled daily at 0000 UTC from the European Centre for Medium-range Weather Forecasts Reanalysis v5 (ERA5), (Hersbach *et al.*, 2020), at 0.25° × 0.25° horizontal resolution. This study uses daily grids over 40 extended summers (DJFM) from 1979–1980 to 2018–2019 for both datasets. A time shift of 1 day has been applied to all rainfall data so that it represents precipitation over the next 24 hr from an indicated time. The 24-hr accumulations of ERA5 rainfall from 0000 UTC have been used in all plots showing synoptic-scale rainfall patterns over Australia and neighbouring oceanic regions, as the AWAP data are only available over Australian land.

2.2 | Synoptic climatology

The synoptic climatology is derived by *k*-means cluster analysis of daily 500 hPa geopotential height anomalies at 0000 UTC over 22°S–54°S and 120°E–170°E, and is the same as that used in Henderson *et al.* (2024). All solutions from $k = 1 \ldots 12$ were tested, and the seven-cluster solution was chosen semi-objectively, on the basis that all clusters are large (>10% of DJFM days) and also reasonably different. For the latter condition, the maximum pattern correlation between any of the cluster centroids is required to be ≤0.6, after Rossow *et al.* (2005). Neither of these thresholds are met when *k* is increased to 8. For $k < 6$, a pattern with an upper trough over southeastern Australia that is important for rainfall over Victoria and Tasmania, which has distinctive Rossby wave breaking characteristics (refer to cluster 6 in Section 4), is not resolved. Furthermore, an annular cluster with a weaker centroid anomaly that emerges when $k = 7$ proves helpful in explaining the differences between heatwave days that affect southern Victoria and Tasmania and those that remain north of the Great Dividing Range in the companion study of Henderson *et al.* (2024).

2.3 | Wet days and heavy rainfall days

Following the convention used by Warren *et al.* (2021) and White *et al.* (2022), a wet day at each grid point is defined as any day on which precipitation over the next 24 hr is ≥1 mm. A heavy rainfall day at a single grid point is then defined as any day on which precipitation exceeds the 95th percentile of wet DJFM days at that grid point over the 40-year period. In Section 3, heavy rainfall is analysed over two subdomains of southeastern Australia, with each enclosing many grid points and having a land area >80,000 km^2. For these subdomains, a "regional heavy rainfall" (RHR) day is any day on which the heavy rainfall criterion is satisfied over grid points that collectively

1477870x, 0, Downloaded from https://rmets.onlinelibrary.wiley.com/doi/10.1002/qj.4936 by Karlsruher Institut Für Technologie, Wiley Online Library on [31/03/2025]. See the Terms and Conditions (https://onlinelibrary.wiley.com/terms-and-conditions) on Wiley Online Library for rules of use; OA articles are governed by the applicable Creative Commons License

represent more than 5% of the land area within its boundary. Latitudinal variation is accounted for in determining the area represented by individual grid points. Days on which this 5%-of-area threshold is not met are referred to as regional non-heavy rainfall (NHR) days.

Wet days occur most frequently along the eastern seaboard and western Tasmania and least frequently in western NSW, northwestern Victoria, and South Australia (Figure 2). Median wet-day rainfall is highest along the eastern seaboard, the Great Dividing Range, and western Tasmania. The 95th percentile of wet-day rainfall is highest over coastal regions of northeastern NSW and southeastern Queensland and the alpine region of northeastern Victoria. While northern South Australia and inland regions of NSW and southern Queensland have a lower frequency of wet days and lower median wet-day rainfall, the 95th percentile is high (typically 30–40 mm), presumably due to tropically influenced convective rainfall. The gap in the gridded data near the Queensland, South Australia, and Northern Territory border results from the sparsity of rain-gauges in this area; (see Jones *et al.*, 2009, their fig. 2).

2.4 | Statistical testing

For each cluster, a two-sample, two-sided test of mean is used to assess the statistical significance of the differences in the composite 500 hPa geopotential height anomalies of r RHR days with those of n NHR days at each grid point. The test consists of 10,000 random shuffles of the $r+n$ dates into two subsets of size r and n, with the null hypothesis of no difference in mean. Variance inflation due to serial correlation in the 500 hPa geopotential height anomalies is accounted for. The first occurrence of the chosen cluster in each DJFM season is treated as being independent; however, subsequent occurrences of that cluster in the same season are only considered to be independent if they fall outside of the decorrelation time from the most recent independent cluster occurrence. Decorrelation times are computed for each grid point by modelling the time series of 500 hPa geopotential height anomalies as an AR(p) process with $1 \leq p \leq 8$, optimised according to the Bayesian information criterion (Wilks, 2006). Allowing for the longer dataset, higher grid resolution, and the inclusion of March in this study, the decorrelation times obtained are consistent with those of Trenberth (1985).

2.5 | Rossby wave breaking

Rossby wave breaking on the 330 K and 350 K isentropic surfaces is computed using a similar method to Song *et al.* (2011). First, longitude intervals that span meridional overturnings of the dynamic tropopause contour (−2 PVU [PV units], where 1 PVU is $10^6\ m^2 \cdot s^{-1} \cdot K \cdot Kg^{-1}$) are identified. Then, the sequence of contour turns (anticlockwise, A, or clockwise, C) made by successive longitude extrema on the overturned contour is used to identify anticyclonic (AC) or cyclonic (CA) wave breaks. The same method was used in Henderson *et al.* (2024), and a more complete description can be found there. The choice of −2 PVU for representing the dynamic tropopause in the Southern Hemisphere is standard (Berrisford *et al.*, 2007; Hoskins & Berrisford, 1988; Pelly & Hoskins, 2003). Nevertheless, the PV surface closest to abrupt shifts from tropospheric to stratospheric air depends on both latitude and season (Hoskins *et al.*, 1985, fig. 1). In Section 4, other PV contours in the neighbourhood of −2 PVU are sometimes plotted when these more effectively mark either Rossby wave breaking or strong meridional perturbations in the vicinity of the dynamic tropopause.

2.6 | Blocking

Blocking is measured using the one-dimensional TMBI (Tibaldi *et al.*, 1994), which uses the 500 hPa geopotential height gradient to identify slow-moving anticyclones. Interested readers can find a detailed description there. The TMBI is used as Pook *et al.* (2013) found that it may identify more episodes of summer blocking near 140°E than the Bureau of Meteorology blocking index used in (Risbey *et al.*, 2009b).

Minor modifications have been made in adopting the TMBI for use with the higher resolution ERA5 dataset. A latitude window of ±5° about the central latitude of 50°S was used to identify blocking at a single longitude, rather than ±3.75°, which was the grid resolution in Tibaldi *et al.* (1994). In their original work, spatial blocking required the single-longitude blocking condition to be satisfied at three consecutive longitudes. At ERA5 grid resolution the same condition would require single-longitude blocking at 31 consecutive longitudes. Instead, the 500 hPa geopotential height has been averaged over 7.5° longitude intervals. The central longitude of each interval is then considered to be spatially blocked if the single-longitude blocking condition is satisfied for the zonally averaged 500 hPa geopotential height field.

Additionally, a persistence criterion requiring spatial blocking over at least five consecutive days has been shortened to 3 days. This was recommended by Schalge *et al.* (2011) for Southern Hemisphere blocking, which is generally shorter-lived than Northern Hemisphere blocking.

1477870x, 0, Downloaded from https://rmets.onlinelibrary.wiley.com/doi/10.1002/qj.4936 by Karlsruher Institut Für Technologie, Wiley Online Library on [31/03/2025]. See the Terms and Conditions (https://onlinelibrary.wiley.com/terms-and-conditions) on Wiley Online Library for rules of use; OA articles are governed by the applicable Creative Commons License

2.7 | Ensemble sensitivity

The ensemble sensitivity technique (Torn & Hakim, 2008) is used in Section 5 to measure spatial relationships between regionally averaged daily rainfall accumulations that have been re-expressed using a symmetry producing Box–Cox power transformation (Wilks, 2006), and precursor anomaly fields of 500 hPa geopotential height, MSLP, averaged 400–600 hPa omega, and precipitable water. A complete description of the ensemble sensitivity technique is provided in Henderson *et al.* (2024).

3 | SYNOPTIC CLIMATOLOGY

The seven-cluster solution of the *k*-means cluster analysis is adopted as the synoptic climatology in both this study and Henderson *et al.* (2024), and a description of the synoptic-scale weather patterns represented by each cluster centroid is provided therein. Clusters 1–5 have more amplified 500 hPa geopotential height anomalies that are arranged zonally (Figure 3), and these can be linked to distinct phases of Rossby wave propagation, whereas the anomalies in clusters 6 and 7 are weaker and resemble meridional dipoles of opposite sign to one another. A diagram and table presenting the frequency of cluster persistence and transitions at a lag of 1 day is provided in Appendix A.

Two of the clusters, cluster 3 and cluster 6, are distinctly wetter over Australian land than the others are (Figures 3 and 4). Clusters 4 and 5 also make a sizeable contribution to heavy rainfall over northeastern NSW and Victoria respectively (Figure 4d,e). These four clusters are briefly described below. Cluster 1 is not analysed even though it accounts for much of the heavy rainfall over western Tasmania (Figure 4a). The rainfall there in this cluster can be largely attributed to orographically forced lifting of the strong west-to-southwesterly flow (Figure 3a).

- **Cluster 3: broad high south of eastern Australia (14.4%)** The positive 500 hPa geopotential height anomaly centred near 51°S, 136°E is the strongest of all the clusters and is accompanied by a strong and broad surface high-pressure system south of eastern Australia (Figure 3c). The location of the surface high-pressure system results in east to southeasterly flow over the eastern seaboard, and positive rainfall anomalies occur throughout NSW and southern Queensland, especially along coastal NSW north of Sydney. The frequency of heavy rainfall days (Figure 4c) is around double the seasonal average over this coastal region (Figure 4h). At a lag of 1 day, the first day of cluster 3 most frequently follows cluster 6 (32%) and cluster 2 (30%).
- **Cluster 4: high in the Tasman Sea (16.3%)** A strong positive 500 hPa geopotential height anomaly lies south of the Tasman Sea with a surface high-pressure system in the Tasman Sea (Figure 3d). This surface-pressure pattern also results in southeasterly flow along much of the eastern seaboard, tending northeasterly along the southern coast of NSW. Positive rainfall anomalies occur along the eastern coast of Australia north of 32°S and the frequency of heavy rainfall days along the northeastern NSW coast is second highest of all the clusters (Figure 4d). The first day in cluster 4 occurs following cluster 3 more than half of the time (54%) and is an important consideration for interpreting the characteristics of heavy rain in these clusters presented in Sections 4 and 5.
- **Cluster 5: Victoria pre-frontal (16.3%)** A pre-frontal trough lies over western Victoria (Figure 3e) with colder air to its southwest. The north to northwesterly flow on its eastern flank is forced to ascend over the Great Dividing Range in central and eastern Victoria and southeastern NSW, resulting in an orographic enhancement to precipitation there. This cluster has the second highest spatial frequency of heavy rainfall days over central-southern Victoria (Figure 4e). Its first day generally follows either clusters 4 or 7 (39% and 35% of the time respectively), and the final day in cluster 5 is followed by cluster 1 on 49% of occasions.
- **Cluster 6: upper trough over southeastern Australia (11.8%)** A negative 500 hPa geopotential height anomaly is centred south of Melbourne near 39°S, 145°E (Figure 3f) and the absolute 500 hPa geopotential height field shows a trough over southeastern Australia—see Henderson *et al.*, 2024, Figure 2f). Slightly downstream, a surface trough is located in the western Tasman Sea, offshore from the coasts of southeastern NSW and eastern Victoria. Although highest rainfall occurs in the southwestern Tasman Sea, the positive composite rainfall anomalies across eastern and southern Victoria, eastern Tasmania, and the southeast of NSW are the largest of all the clusters. The frequency of heavy rainfall days (Figure 4f) is the highest of all the clusters for southern Victoria and eastern Tasmania. Cluster 4 (38%) and cluster 5 (27%) are the most common precursors to the first day in cluster 6 at a lag of 1 day.

Clusters 2 and 7 are generally drier across southeastern Australia (Figure 3b,g), and heavy rainfall frequency is either less than the seasonal average or close to the seasonal average in the case of northeastern NSW and southeastern Queensland (Figure 4b,g,h).

1477870x, 0, Downloaded from https://rmets.onlinelibrary.wiley.com/doi/10.1002/qj.4936 by Karlsruher Institut Für Technologie, Wiley Online Library on [31/03/2025]. See the Terms and Conditions (https://onlinelibrary.wiley.com/terms-and-conditions) on Wiley Online Library for rules of use; OA articles are governed by the applicable Creative Commons License

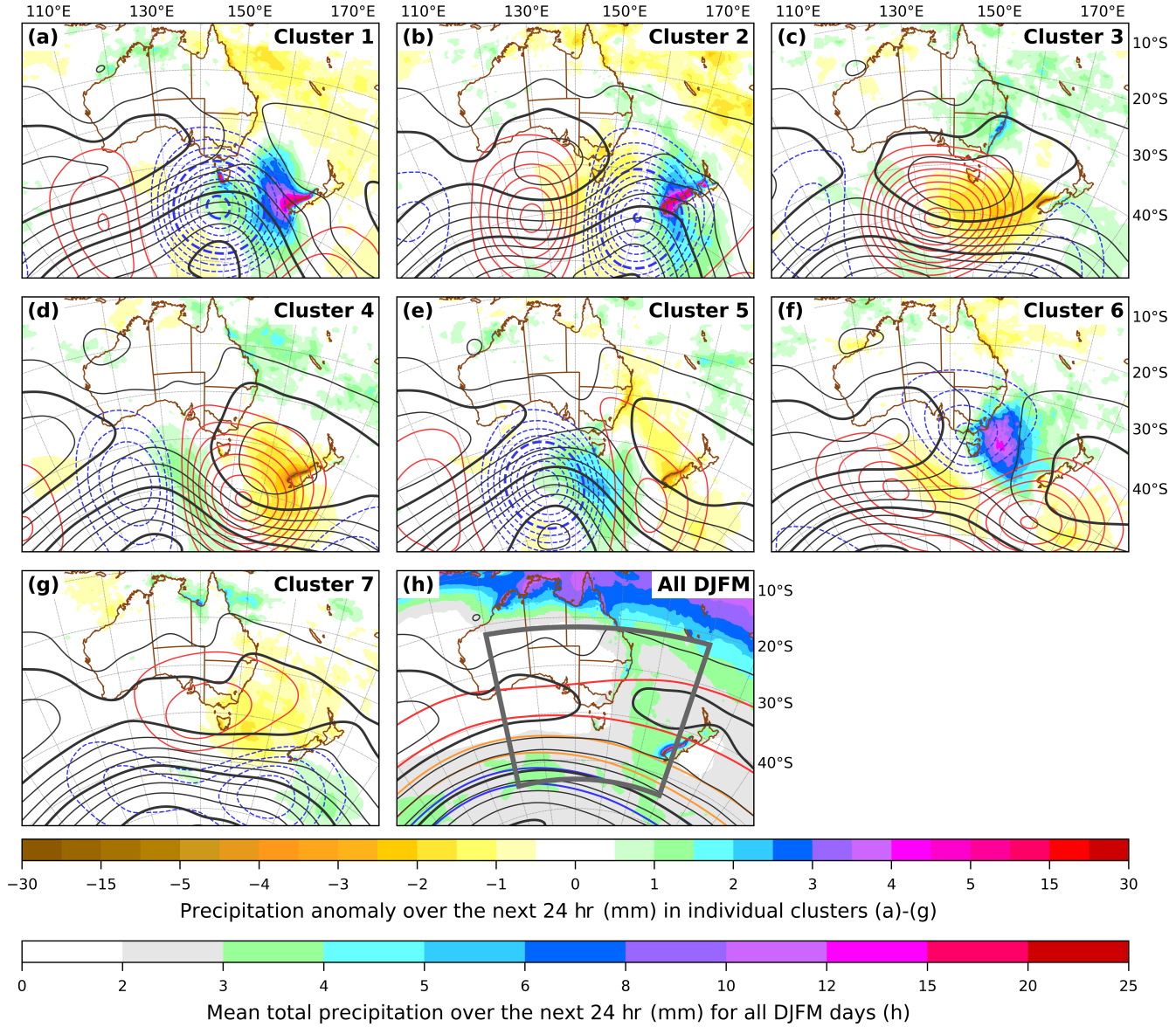

FIGURE 3 (a)–(g) Cluster centroids at 0000 UTC of precipitation anomalies over the next 24 hr (fill), 500 hPa geopotential height anomalies (contours every 20 gpm with red positive, blue dashed negative, and bold every 100 gpm), and absolute mean-sea-level pressure (MSLP; black contours every 4 hPa, with bold contours every 16 hPa for ≤1,016 hPa, decreasing poleward). (h) Mean absolute fields at 0000 UTC for all December–March (DJFM) days of next 24-hr rainfall (fill), MSLP (black contours as previously described), and 500 hPa geopotential height (coloured contours every 100 gpm with a northern red contour of 5,800 gpm, decreasing poleward). The grey boundary is the spatial domain over which the cluster analysis was performed. [Colour figure can be viewed at wileyonlinelibrary.com]

The highest rainfall in southeastern Australia occurs along the northern coast of eastern NSW north of 33°S, as seen in Figures 2, 3h, and 4h. Accordingly, a subdomain covering this rainfall maximum, labelled NEC, is constructed to compare RHR days with NHR days in its wettest pattern, Cluster 3 (Figures 3c and 4c). For central and eastern parts of southern Victoria, and eastern Tasmania, the highest rainfall occurs in cluster 6 (Figures 3f and 4f). A second subdomain, labelled SVT, is constructed to study RHR and NHR days in this cluster. However, this subdomain excludes western Tasmania to minimise the number of RHR days that fall into cluster 1. These two clusters have very different synoptic patterns: the rainfall in western Tasmania in cluster 1 (Figures 3a and 4a) is heavily influenced by orographic forcing in westerly flows, whereas the surface flow in cluster 6 is meridional and often has an easterly component. The NEC and SVT subdomains have similar land areas, and roughly one-sixth of days in their wettest cluster, 3 and 6 respectively, is an RHR day (Table 1).

1477870x, 0, Downloaded from https://rmets.onlinelibrary.wiley.com/doi/10.1002/qj.4936 by Karlsruher Institut Für Technologie, Wiley Online Library on [31/03/2025]. See the Terms and Conditions (https://onlinelibrary.wiley.com/terms-and-conditions) on Wiley Online Library for rules of use; OA articles are governed by the applicable Creative Commons License

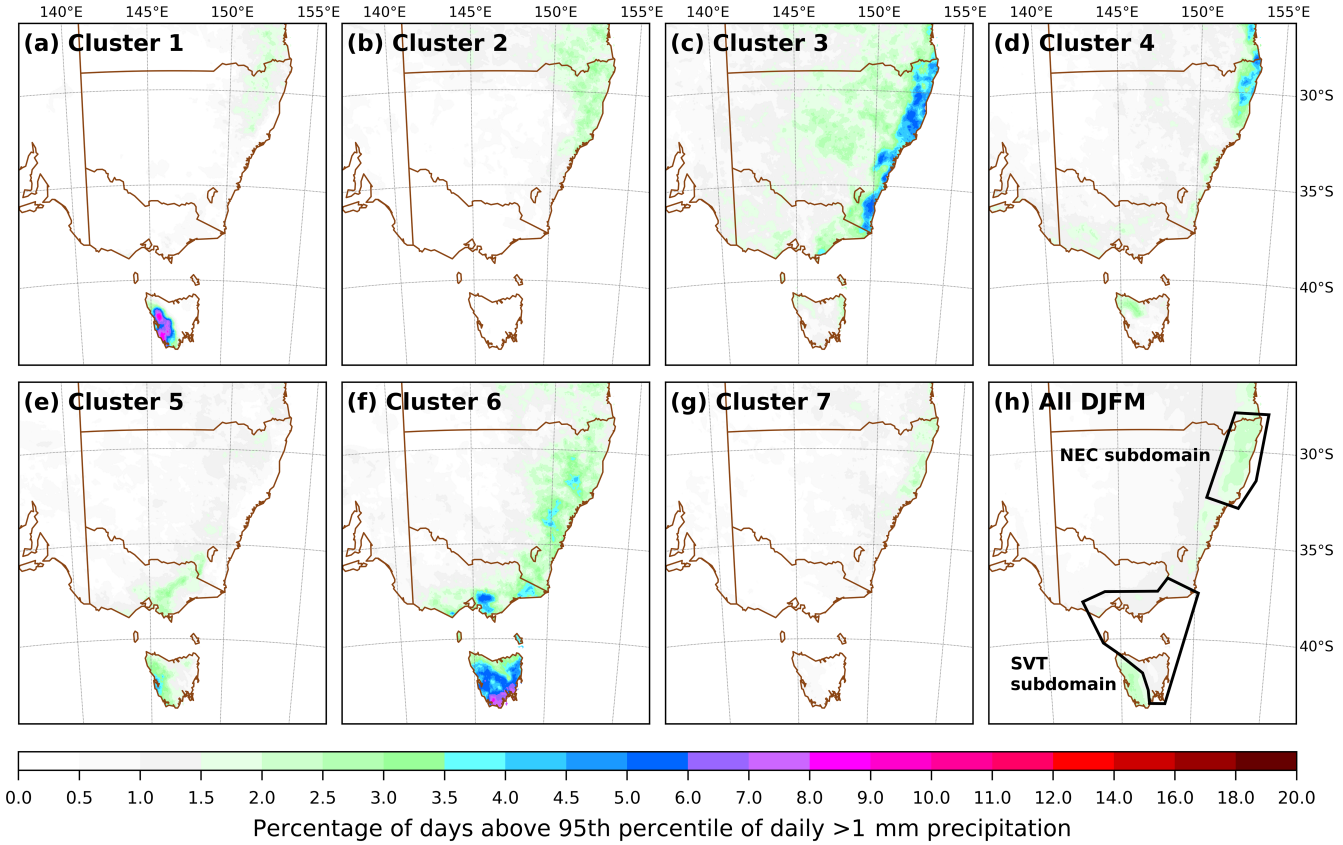

FIGURE 4 Percentage of days (a)–(g) above the 95th percentile of December–March (DJFM) wet-day (≥1 mm) precipitation in each cluster and (h) for all DJFM days. Black polygons in (h) show the northern coast of eastern New South Wales (NEC) and southern Victoria and eastern Tasmania (SVT) subdomains. [Colour figure can be viewed at wileyonlinelibrary.com]

TABLE 1 Descriptions of subdomains used with the two wettest clusters and the number (percentage) of regional heavy rainfall (RHR) and regional non-heavy rainfall (NHR) days for each subdomain in the corresponding cluster.

Cluster	Weather state	Subdomain with large percentage of RHR days	Label	RHR days	NHR days
3	Broad high	Northeastern coast of New South Wales	NEC	105 (15.0%)	595 (85.0%)
6	Upper trough	Southern Victoria and eastern Tasmania	SVT	97 (17.0%)	474 (83.0%)

RHR days account for 46% of total area-averaged DJFM precipitation in the NEC subdomain and 44% in the SVT subdomain. A single RHR day, or two consecutive RHR days, accounts for 66% and 78% of RHR days in the NEC and SVT subdomains respectively. The longest run of six consecutive RHR days in the NEC subdomain occurred from January 12 to 17, 2009, with every single day falling in cluster 3. The number of RHR days in the NEC and SVT subdomains for each cluster is shown in Table 2. Clusters 3 and 4 together account for 45% of RHR days over the NEC subdomain, with these RHR days making up 23% of its total DJFM precipitation. Clusters 3, 4, 5, and 6 account for nearly 90% of RHR days over the SVT subdomain, with these RHR days comprising 40% of its total DJFM precipitation. Accordingly, the comparison of RHR days with NHR days will focus on clusters 3 and 4 for the NEC subdomain and on clusters 5 and 6 for the SVT subdomain.

4 | COMPARISON OF RHR AND NHR DAYS

In this section, the mean properties of RHR days are compared with those of NHR days in the NEC and SVT subdomains using composite and difference plots. Hovmöller diagrams showing upper tropospheric Rossby wave propagation and breaking, midtropospheric vertical motions, and blocking at 500 hPa are also presented for selected clusters. Day 0 in each Hovmöller plot corresponds to the day of the RHR and NHR composites.

1477870x, 0, Downloaded from https://rmets.onlinelibrary.wiley.com/doi/10.1002/qj.4936 by Karlsruher Institut Für Technologie, Wiley Online Library on [31/03/2025]. See the Terms and Conditions (https://onlinelibrary.wiley.com/terms-and-conditions) on Wiley Online Library for rules of use; OA articles are governed by the applicable Creative Commons License

TABLE 2 Number of regional heavy rainfall (RHR) days in each cluster for the northern coast of eastern New South Wales (NEC) and southern Victoria and eastern Tasmania (SVT) subdomains, the total number of RHR days (percentage of December–March [DJFM] days) for each subdomain, and the mean area-averaged wet-day rainfall taken over all days in the cluster.

Cluster	1	2	3	4	5	6	7	All DJFM
NEC subdomain RHR days	30	57	105	80	33	55	51	411 (8.47%)
Mean wet-day rainfall (mm)	3.2	4.6	6.9	5.1	2.4	4.9	3.6	4.4
SVT subdomain RHR days	15	5	70	50	57	97	14	308 (6.35%)
Mean wet-day rainfall (mm)	1.8	0.5	1.9	1.6	2.1	3.8	0.7	1.7

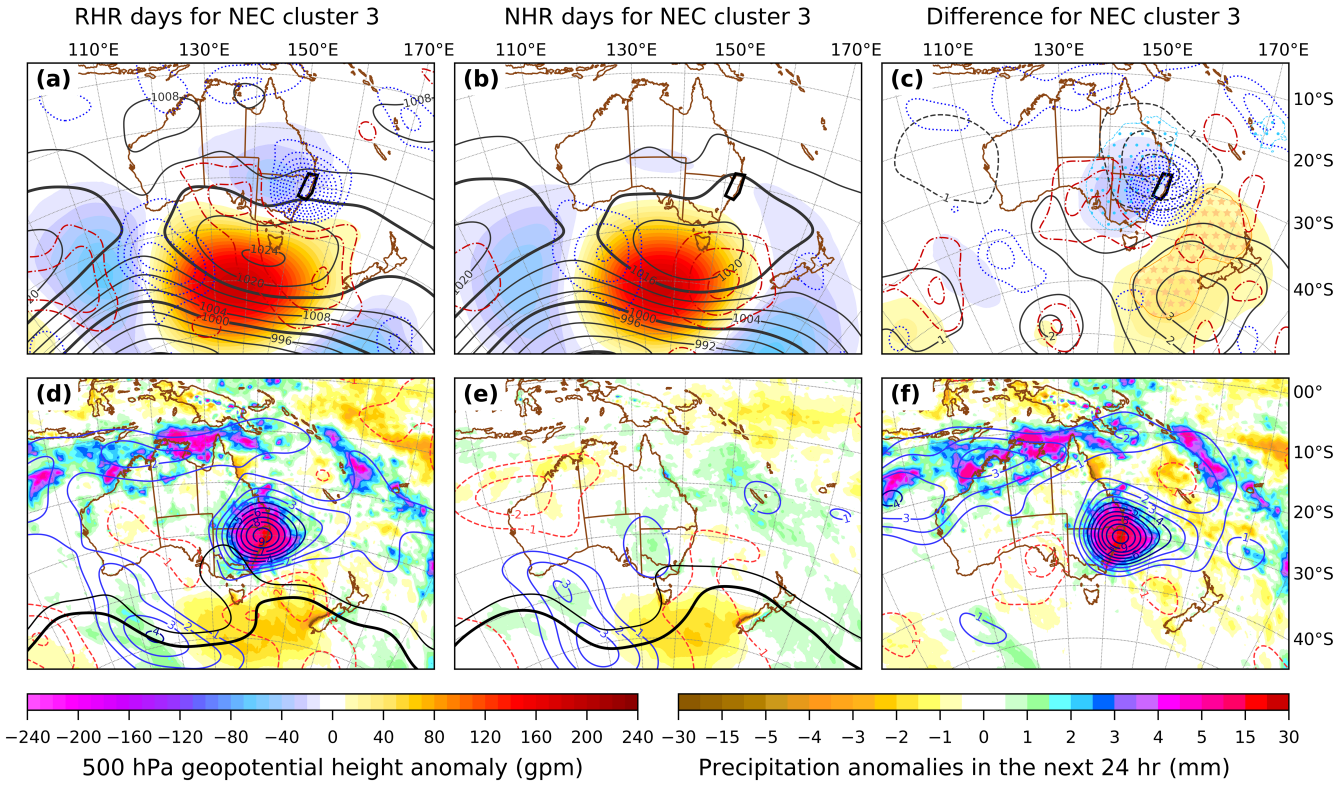

FIGURE 5 (a)–(c) The 500 hPa geopotential height anomalies (fill), absolute mean-sea-level pressure (MSLP; black contours), and 400–600 hPa averaged omega vertical velocity anomalies (red dash-dot contours positive and blue dotted contours negative) for (a) regional heavy rainfall (RHR) days and (b) regional non-heavy rainfall (NHR) days in cluster 3, northern coast of eastern New South Wales (NEC) subdomain (black polygon). MSLP contour intervals in (a) and (b) are as per Figure 3. The omega anomalies are contoured every 0.02 Pa· s^{-1} with the zero contour omitted. The difference, (a) minus (b), is shown in (c) with MSLP contours every 1 hPa, negative dashed, zero omitted, and bold every ±4 hPa. Orange star (light blue dot) stippling in (c) shows regions where the RHR day composite 500 hPa geopotential height anomaly is greater than (less than) the NHR day composite with statistical significance above the 95% confidence level. (d)–(f) As per (a)–(c) but for anomalies of 24-hr precipitation (fill) and precipitable water (contours). Contour interval is 1 mm with positive blue, negative dashed red, and zero omitted. Solid black contours in (d) and (e) are the −2 PVU (bold) and −1.5 PVU contours of potential vorticity (PV) at 330 K. [Colour figure can be viewed at wileyonlinelibrary.com]

4.1 | Cluster 3, NEC subdomain

A negative 500 hPa geopotential height composite anomaly lies over NSW and southern Queensland on RHR days (Figure 5a) on the northern flank of an anticyclonically breaking Rossby wave (the meridional overturning of the 330 K PV contours in Figure 5d). As the former is consistent with either an upper trough or cut-off low aloft (see Barnes *et al.*, 2023, figs. 1 and 2), the term "cut-off upper cyclonic anomaly" will be used to describe all negative 500 hPa geopotential height anomalies that are flanked to their south by a positive 500 hPa geopotential height anomaly throughout their longitudinal extent. The cut-off upper cyclonic anomaly is absent from the NHR

1477870x, 0, Downloaded from https://rmets.onlinelibrary.wiley.com/doi/10.1002/qj.4936 by Karlsruher Institut Für Technologie, Wiley Online Library on [31/03/2025]. See the Terms and Conditions (https://onlinelibrary.wiley.com/terms-and-conditions) on Wiley Online Library for rules of use; OA articles are governed by the applicable Creative Commons License

composite, save for a smaller and weaker anomaly near the border of South Australia and the Northern Territory (Figure 5b), and the perturbation to the dynamic tropopause is smaller (Figure 5e). The positive 500 hPa geopotential height anomaly south of mainland Australia on RHR days is broader and extends further east across the Tasman Sea.

Lower geopotential height over south and central eastern Australia and higher geopotential height over the eastern Tasman Sea are statistically significant features of RHR days (Figure 5c). Nevertheless, there are cases of comparably strong cut-off upper cyclonic anomalies over NSW on some of the NHR days. These are not as apparent in the NHR composite though, due to (a) being averaged over a larger number of cases, most of which have weaker negative anomalies, and (b) their local 500 hPa geopotential height minima (and hence, their area of greatest rainfall) being displaced a greater distance from the northern coast of eastern NSW than those of the RHR days. Similar limitations also apply to the other cluster and subdomain cases presented in this study.

The sequence of positive and negative midtropospheric omega anomalies upstream of the upper trough on RHR days is consistent with a propagating Rossby Wave. However, the splitting of the flow west of Bass Strait with two separate maxima in the subsiding anomaly—an equatorward branch to the west of the cut-off upper cyclonic anomaly over southeastern Australia, and a poleward branch in the southern Tasman Sea on the eastern flank of the surface high pressure system (Figure 5a)—is also consistent with the signature of anticyclonic Rossby wave breaking in Figure 5d. Only the poleward subsiding branch is evident on NHR days (Figure 5b). By construction, a strong positive rainfall anomaly lies directly over the NEC subdomain on RHR days (Figure 5d,f). This is co-located with a similarly shaped region of strong midtropospheric ascent and a slightly larger precipitable water maximum that extends east across the northern Tasman Sea. A ribbon of enhanced vertically integrated water vapour flux is directed west to southwest towards the NEC subdomain (not shown) and aligns closely with this precipitable water maximum. In comparison, mean rainfall and humidity over the northeastern coast of NSW on NHR days differs little from the climatological average (Figure 5e), and an enhanced water vapour flux is directed to the northwest along the central-eastern coast of Queensland (not shown).

On NHR days, the surface high-pressure system south of mainland Australia extends a ridge along the NSW coast. The resulting geostrophic flow along the eastern seaboard is east to southeasterly (Figure 5b), whereas, for RHR days, the lower surface pressure over eastern Australia and higher surface pressure south of New Zealand (Figure 5a,c) sets up easterly geostrophic flow over the eastern seaboard. These differences in the surface-pressure patterns over the eastern Australian coast are similar to those reported by Black and Lane (2015) for high- and low-rainfall days. Their finding of a relationship between eastern-seaboard rainfall and increased easterly flow with midtropospheric ascent is well explained by the surface pressure and vertical motion differences that result from the presence of a nearby cut-off upper cyclonic anomaly to the west in this cluster.

Precipitable water and convection is higher in the Australian Tropics on RHR days (Figure 5d–f), and midtropospheric ascent is occurring over much of this region (Figure 5a,c). The lead-up to RHR days over the NEC subdomain in cluster 3 (Figure 6) shows active tropical convection on day −6. The humid airmass and convection then extend across Australia from northwest to the southeast on day −4, continuing to day −2 when the upper cyclonic anomaly begins to form. However, no relationship was found between RHR days in cluster 3 and phases of the Madden–Julian oscillation at lead times of up to 6 days. This may indicate that the tropical convection preceding RHR days is linked to the equatorward propagation of midlatitude Rossby waves (e.g. Berry *et al.*, 2012; Narsey *et al.*, 2017; O'Brien & Reeder, 2017).

Enhanced blocking from 135°E to 160°E is a prominent feature of RHR days in cluster 3 (Figure 7a). It is the key difference with NHR days (Figure 7b), even though spatial correlations between blocking at 140°E and overall summer rainfall in southeastern Australia are weak (Risbey *et al.*, 2009b). The blocking occurs downstream of anticyclonic Rossby wave breaking at Australian longitudes, with the latter initiating up to 2 days *before* the onset of heavy rain (Figure 7). The upper cut-off cyclonic anomaly and evidence of split flow in the composite for heavy rainfall days (Figure 5a) are consistent with increased blocking. Unlike the anticyclonic Rossby wave breaking, the blocking frequency peaks at day +1, the day *following* the composite heavy rain. In the week following the blocking on RHR days, cyclonic Rossby wave breaking sometimes occurs between 135°E and 170°W.

Anticyclonic Rossby wave breaking prior to downstream blocking also occurs on NHR days; however, the frequency of both phenomena is considerably lower and their regions of peak frequency are shifted around 15° further east than those of RHR days. The blocking between 180° and 150°W in the lead-up to NHR days is close to the climatological average (these longitudes have the highest frequency of blocking). However, it is noteworthy that blocking is not common at these longitudes after the occurrence of cluster 3, unless it is preceded by heavy rainfall over southeastern Australia. It is likely that the tropical convection occurring in the lead-up to RHR days

1477870x, 0, Downloaded from https://rmets.onlinelibrary.wiley.com/doi/10.1002/qj.4936 by Karlsruher Institut Für Technologie, Wiley Online Library on [31/03/2025]. See the Terms and Conditions (https://onlinelibrary.wiley.com/terms-and-conditions) on Wiley Online Library for rules of use; OA articles are governed by the applicable Creative Commons License

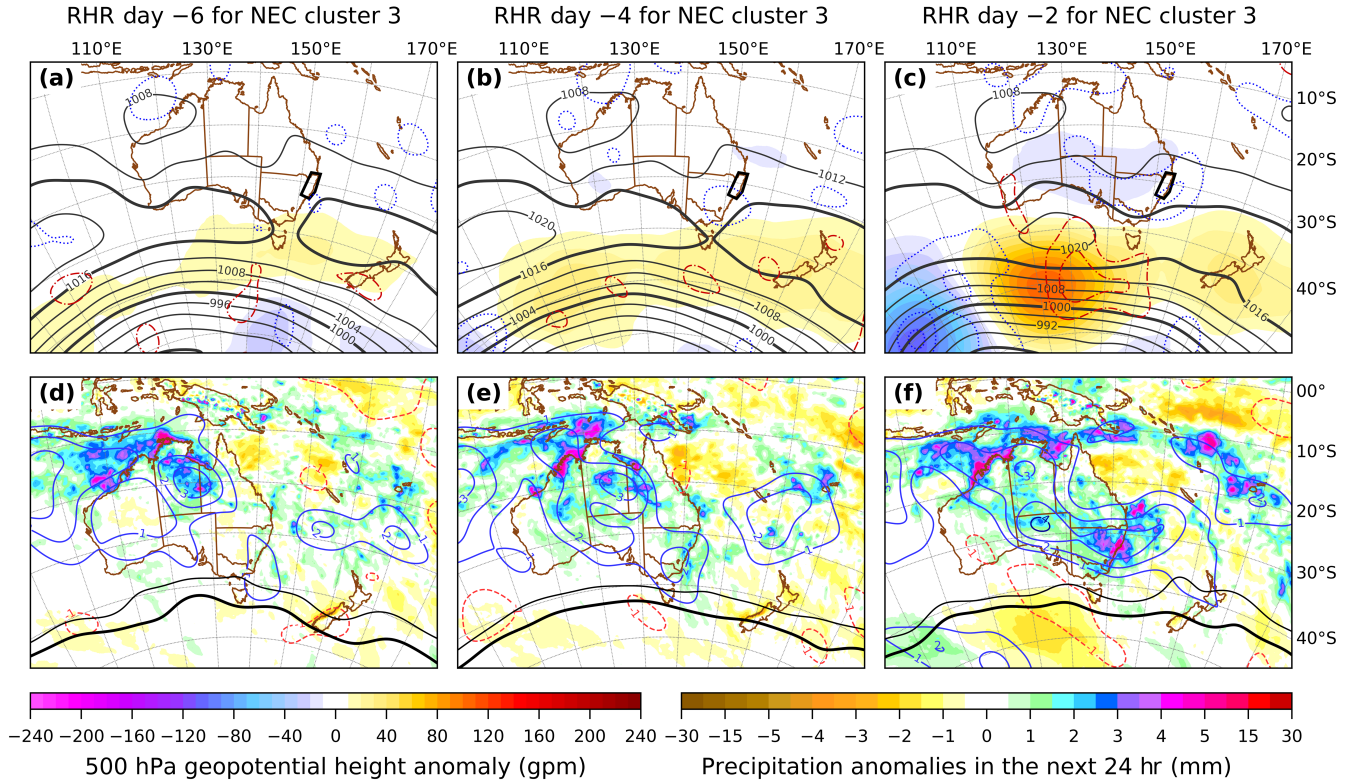

FIGURE 6 (a)–(c) Cluster 3, northern coast of eastern New South Wales (NEC) subdomain, regional heavy rainfall (RHR) cases as per Figure 5a, but instead for (a) day −6, (b) day −4, and (c) day −2. (d)–(f) Same, but as per Figure 5d. [Colour figure can be viewed at wileyonlinelibrary.com]

(Figure 6d–f) is contributing to the enhanced anticyclonic Rossby wave breaking at Australian longitudes prior to RHR days (see Section 4.4).

Heavy rainfall days in cluster 3 were also tested with other subdomains, including SVT, western NSW, and southeastern NSW. The results (not shown) are very similar, even though only 10% of RHR days in the NEC subdomain are also RHR days in the SVT subdomain. In each case, a cut-off upper cyclonic anomaly lies immediately to the west of the subdomain. This feature is either absent or substantially weaker on NHR days.

4.2 | Cluster 4, NEC subdomain

The second largest number of RHR days over the NEC subdomain occurs in cluster 4, including its wettest day during the 40-year period studied. Area-mean rainfall over the entire NEC subdomain exceeded 100 mm in the 24 hr to 0900 h local time on January 28, 2013, an event that was associated with ex-Tropical Cyclone *Oswald*. There are clear similarities with RHR days in cluster 3. A cut-off upper cyclonic anomaly is situated northwest of the NEC subdomain with strong ascending motion over the subdomain (Figure 8a–c). Once again, a stronger positive 500 hPa geopotential height anomaly lies in the eastern Tasman Sea in comparison with NHR days. The combination of negative surface-pressure anomalies over and to the north of the NEC subdomain, and higher surface pressure in the southern Tasman Sea, results in east to northeasterly flow over the NEC subdomain. The pattern for RHR days in cluster 4 is very similar to that of the heavy rain event of February 23, 2022, discussed in Barnes *et al.* (2023, their fig. 1). Though both RHR and NHR subsets have a high-pressure system in the Tasman Sea, there is no composite upper cyclonic anomaly or ascending motion near the NEC subdomain on NHR days. As with cluster 3, a surface ridge extends from the Tasman Sea over the Queensland coast on NHR days, resulting in east to southeasterly geostrophic flow.

Maximum rainfall is co-located with maximum ascent and occurs over the northern half of the subdomain (Figure 8d–f), a degree or two further north than with cluster 3. Likewise, the precipitable water maximum on RHR days extends farther afield than the rainfall maximum and is again radially symmetric about the NEC subdomain. An enhanced flux of water vapour from the Coral Sea towards the NEC subdomain (not shown) is largely confined to the region of the precipitable water maximum in

1477870x, 0, Downloaded from https://rmets.onlinelibrary.wiley.com/doi/10.1002/qj.4936 by Karlsruher Institut Für Technologie, Wiley Online Library on [31/03/2025]. See the Terms and Conditions (https://onlinelibrary.wiley.com/terms-and-conditions) on Wiley Online Library for rules of use; OA articles are governed by the applicable Creative Commons License

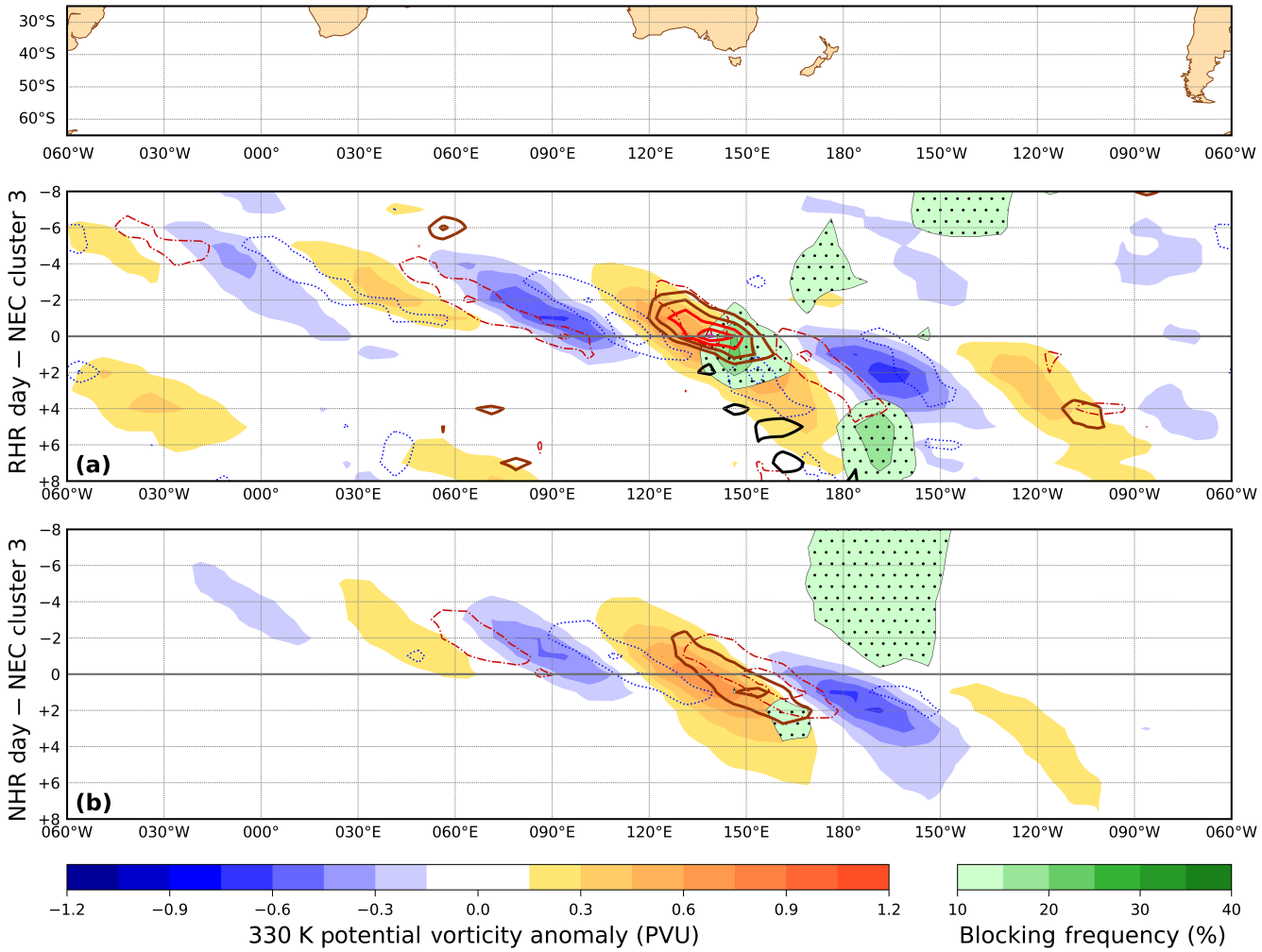

FIGURE 7 Composite of 330 K potential vorticity (PV) anomalies (fill), Tibaldi–Molteni blocking index (TMBI; fill with contours and dot stippling), anticyclonic Rossby wave breaking at 330 K (thick coloured contours), cyclonic Rossby wave breaking at 330 K (thick black contours) and 400–600 hPa averaged omega vertical velocity anomalies (thin contours with red dash-dot positive, blue dotted negative, zero omitted) in cluster 3, northern coast of eastern New South Wales (NEC) domain for (a) regional heavy rainfall (RHR) days and (b) non-heavy rainfall (NHR) days. The PV, Rossby wave breaking, and omega fields are averaged over the latitudes of 24°S–66°S. Daily fields making up all composites are averaged over 7.5° longitude intervals, except for TMBI, where the maximum value (0 or 1 at each grid point) is taken over the interval. Anticyclonic Rossby wave breaking frequency is divided by its December–March climatological value to emphasise wave breaking at longitudes near eastern Australia, and these contours are multiples of the climatological frequency ≥2.0 at intervals of 0.5. Cyclonic wave breaking contours are the absolute frequency ≥2.0% at intervals of 0.5%. Time is shown increasing downwards, with day 0 representing the composite dates of the RHR and NHR subsets. [Colour figure can be viewed at wileyonlinelibrary.com]

Figure 8d, but otherwise it has a similar spatial distribution to the integrated vapour transport field shown in Barnes *et al.* (2023, their fig. 1c). The main difference with cluster 3 occurs over northern Australian, which is much drier in cluster 4 and has subsiding motion over central-northern Australia and western Queensland. In cluster 4, the upper trough and heavy rainfall over the region are already evident 2 days beforehand (not shown) and cluster 3 RHR days occur on the day prior to cluster 4 RHR days on 25% of occasions.

Once again, enhanced anticyclonic Rossby wave breaking occurs *prior to* RHR days (Figure 9a), but the peak anticyclonic Rossby wave breaking frequency occurs farther east than in cluster 3. Though the subsequent blocking is evident at Tasman Sea longitudes the day before the onset of heavy rainfall, peak blocking frequency occurs between 165°E and 165°W at least 1 day *after* the composite heavy rain. The peak blocking frequency east of 180° occurs 1–5 days after a second peak in anticyclonic Rossby wave breaking near 170°E on the day that composite heavy rain falls in the western Tasman Sea (Figure 8d,f). This is well above the climatological blocking frequency, with the latter very similar to the blocking frequency there prior to NHR days (Figure 9b).

1477870x, 0, Downloaded from https://rmets.onlinelibrary.wiley.com/doi/10.1002/qj.4936 by Karlsruher Institut Für Technologie, Wiley Online Library on [31/03/2025]. See the Terms and Conditions (https://onlinelibrary.wiley.com/terms-and-conditions) on Wiley Online Library for rules of use; OA articles are governed by the applicable Creative Commons License

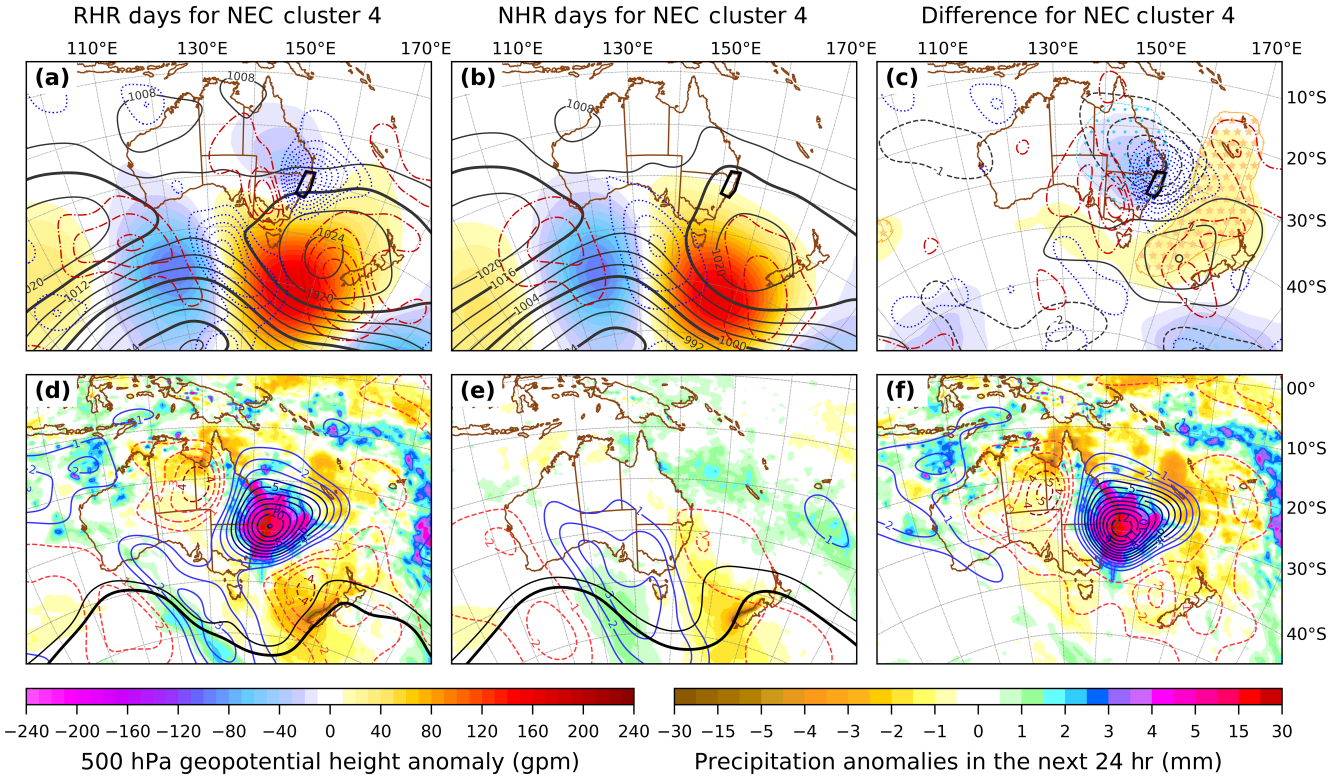

FIGURE 8 As per Figure 5 but for cluster 4, northern coast of eastern New South Wales (NEC) subdomain. [Colour figure can be viewed at wileyonlinelibrary.com]

On the majority of dates that cluster 4 first occurs, a strong high-pressure system enters the Tasman Sea from cluster 3 the day beforehand. In both clusters, the heavy rain develops a couple of days after the initiation of anticyclonic Rossby wave breaking. As the two clusters frequently appear in this same sequence in multi-day episodes of heavy rain, it is apparent that their distinctive feature in comparison with NHR days is a slow-moving cut-off upper cyclonic anomaly (Barnes *et al.*, 2023).

4.3 | Cluster 6, SVT subdomain

Five of the top 10 wettest days over the SVT subdomain in the 40-year period occurred in cluster 6, including its wettest 24 hr to 0900 h local time on February 3, 2005.

An upper cut-off cyclonic anomaly and a positive 500 hPa geopotential height anomaly to its southeast in the Tasman Sea (Figure 10a–c) are statistically significant features that are also seen with RHR days for the NEC subdomain in clusters 3 and 4. In comparison, the upper cut-off cyclonic anomaly is deeper for the SVT subdomain in cluster 6 and the subsidence upstream and ascent downstream of it are stronger. Poleward of the upper cut-off cyclonic anomaly, the positive geopotential height anomaly extends farther west than the previous cases, as far as 110°E. The 500 hPa geopotential height anomalies are stronger on RHR days than on NHR days, and the upper cut-off cyclonic anomaly is centred further northwest over southwestern Victoria. Composite cyclonic Rossby wave breaking at 330 K occurs near 150°E on RHR days, but not on NHR days (as indicated by the 330 K PV contours in Figure 10d,e). Otherwise, their upper tropospheric patterns are similar. Surface pressure is lower over Victoria and Tasmania on RHR days. These show a composite closed surface low-pressure system centred over central-eastern Bass Strait, compared with a weaker open trough in the western Tasman Sea on NHR days.

The stronger anomalies in the pressure pattern and more northwestward proximity of the upper cut-off cyclonic anomaly result in heavier rainfall over the SVT subdomain and the western Tasman Sea (Figure 10d–f). On NHR days, positive rainfall anomalies are more confined to the Tasman Sea. Air over the Coral Sea and Gulf of Carpentaria on RHR days is anomalously dry and coincident with regions of subsidence, but increased precipitable water and rainfall occur over northwestern Australia. A similar rainfall and moisture distribution over the Australian Tropics is seen throughout the days leading up to SVT heavy rainfall days in Figure 11. The upper cyclonic anomaly that is associated with heavy rainfall lies south of the Great Australian Bight 2 days earlier. This is preceded

1477870x, 0, Downloaded from https://rmets.onlinelibrary.wiley.com/doi/10.1002/qj.4936 by Karlsruher Institut Für Technologie, Wiley Online Library on [31/03/2025]. See the Terms and Conditions (https://onlinelibrary.wiley.com/terms-and-conditions) on Wiley Online Library for rules of use; OA articles are governed by the applicable Creative Commons License

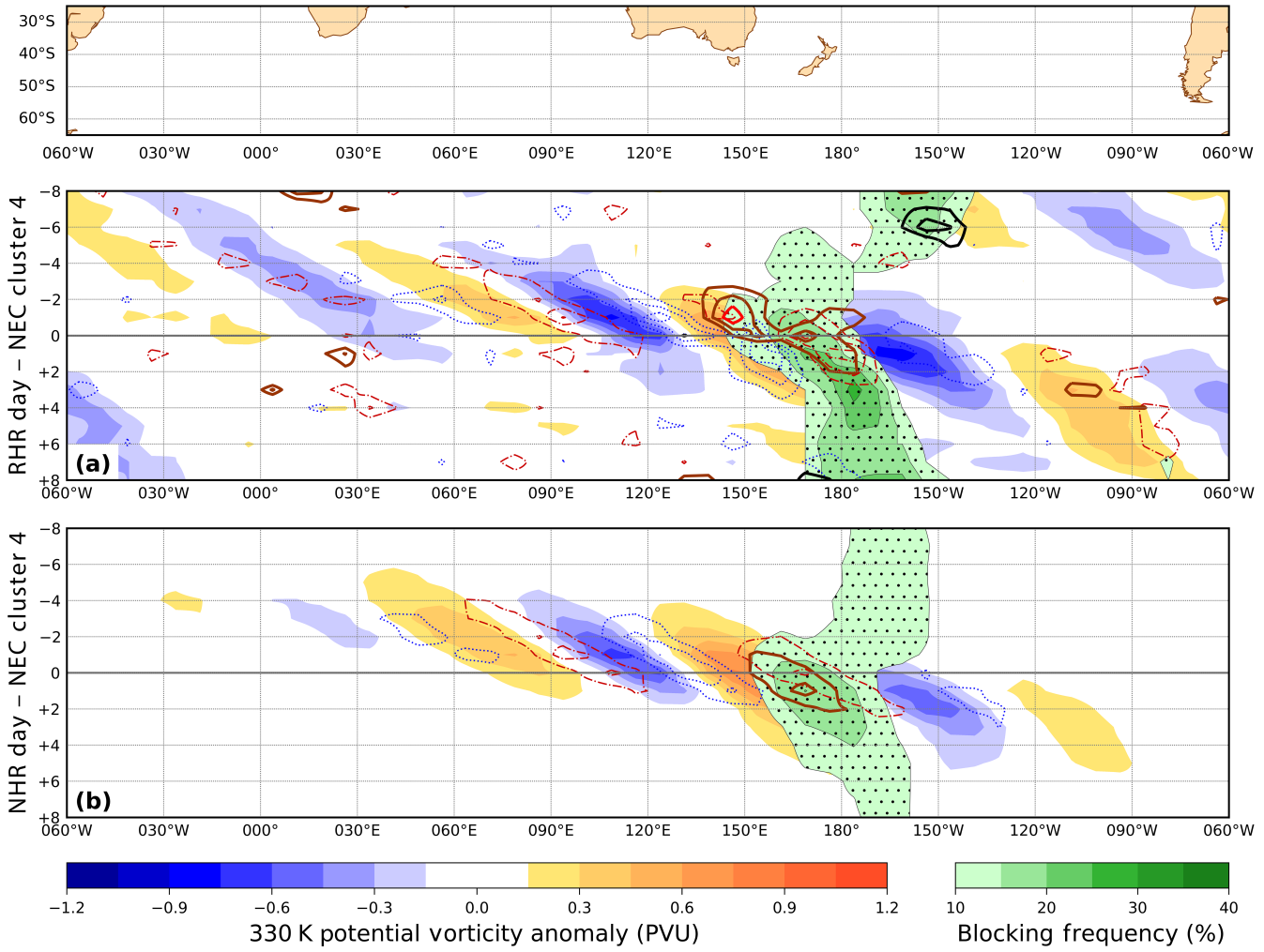

FIGURE 9 As per Figure 7 but for cluster 4, northern coast of eastern New South Wales (NEC) subdomain. [Colour figure can be viewed at wileyonlinelibrary.com]

by an upper cyclonic anomaly over NSW on day −4 that is associated with increased rainfall on the eastern seaboard. The plume of precipitable water extending from Western Australia to NSW on day −6 is somewhat similar to the moisture distribution for the NEC subdomain in cluster 3 on day −4 and day −2 (Figure 6). In the 6 days prior to cluster 6 RHR days, a cluster 3 RHR day occurs in the NEC subdomain 19% of the time.

In comparison with NHR days, PV anomalies at 330 K are stronger in the lead-up to RHR days (Figure 12), consistent with their stronger 500 hPa geopotential height anomalies in Figure 10. As with the other cases seen so far, enhanced anticyclonic Rossby wave breaking in the 2 days before the composite heavy rainfall is a key characteristic that distinguishes RHR days from NHR days. Similar to the RHR cases in the NEC subdomain, high blocking frequencies develop *following* anticyclonic Rossby wave breaking with a local maximum between 135°E and 160°E from day −1 to day +4, that peaks near 155°E 1–2 days *after* RHR days.

Cluster 6 has some unique characteristics, including the high frequency of blocking between 180° and 150°W from 7 days prior to 3 days afterwards (Figure 12) and a peak in cyclonic Rossby wave breaking frequency after day 0 that is far higher than all the other clusters. The negative 500 hPa geopotential height anomaly over southeastern Australia in this cluster (Figure 3f) creates a cyclonic shear on the 500 hPa surface equatorward of the mean midlatitude jet (Figure 3h). The addition of cyclonic shear equatorward of the jet is consistent with baroclinic life cycles with cyclonic rather than anticyclonic Rossby wave breaking (Peters & Waugh, 1996; Thorncroft *et al.*, 1993). In cluster 6, the implied cyclonic shear is stronger on RHR days than on NHR days (Figure 10), and this coincides with a higher subsequent cyclonic Rossby wave breaking frequency (Figure 12). Thorncroft *et al.* (1993) showed that the peak eddy kinetic energy of the cyclonically breaking LC2 baroclinic life cycle is higher than that of the anticyclonically breaking LC1 life cycle, and remains high for considerably longer. This result may explain

1477870x, 0, Downloaded from https://rmets.onlinelibrary.wiley.com/doi/10.1002/qj.4936 by Karlsruher Institut Für Technologie, Wiley Online Library on [31/03/2025]. See the Terms and Conditions (https://onlinelibrary.wiley.com/terms-and-conditions) on Wiley Online Library for rules of use; OA articles are governed by the applicable Creative Commons License

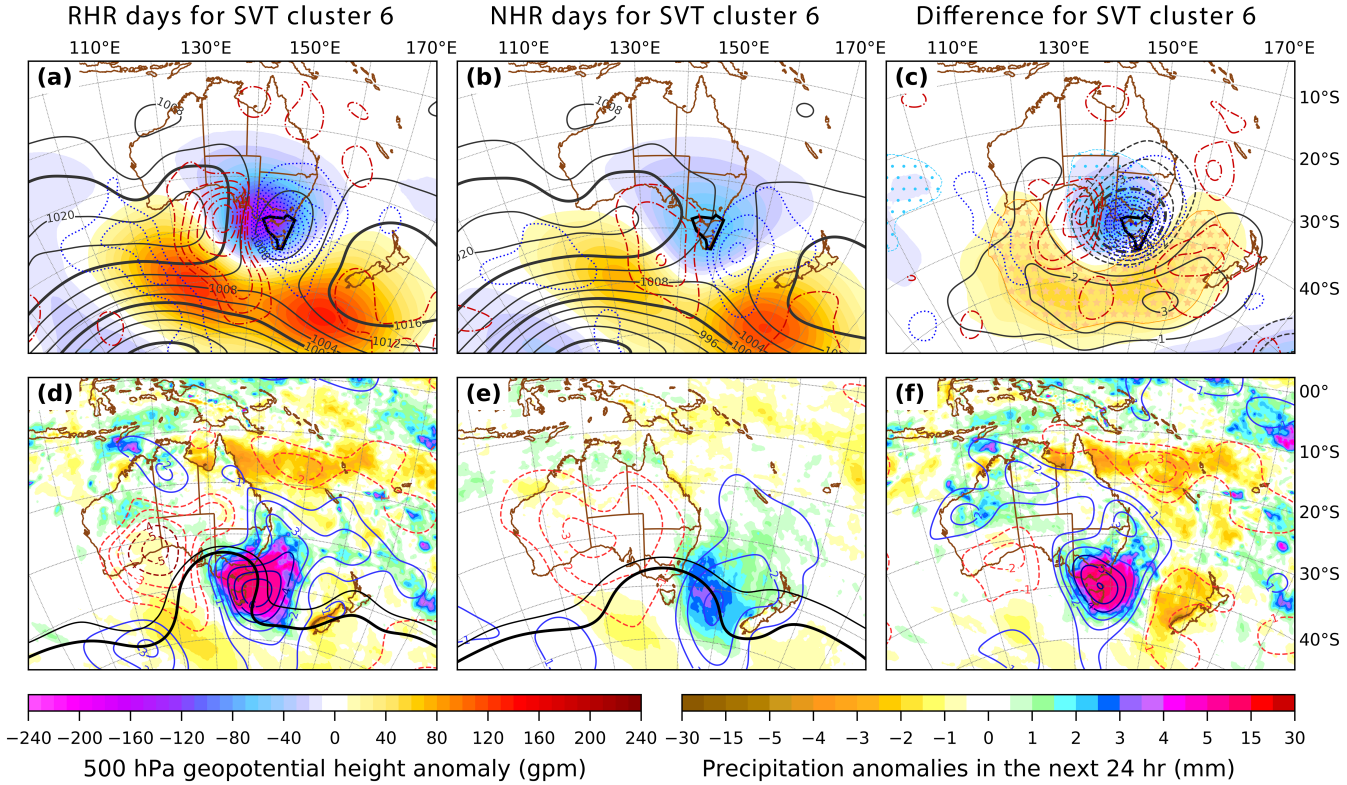

FIGURE 10 As per Figure 5 but for cluster 6, southern Victoria and eastern Tasmania (SVT) subdomain. [Colour figure can be viewed at wileyonlinelibrary.com]

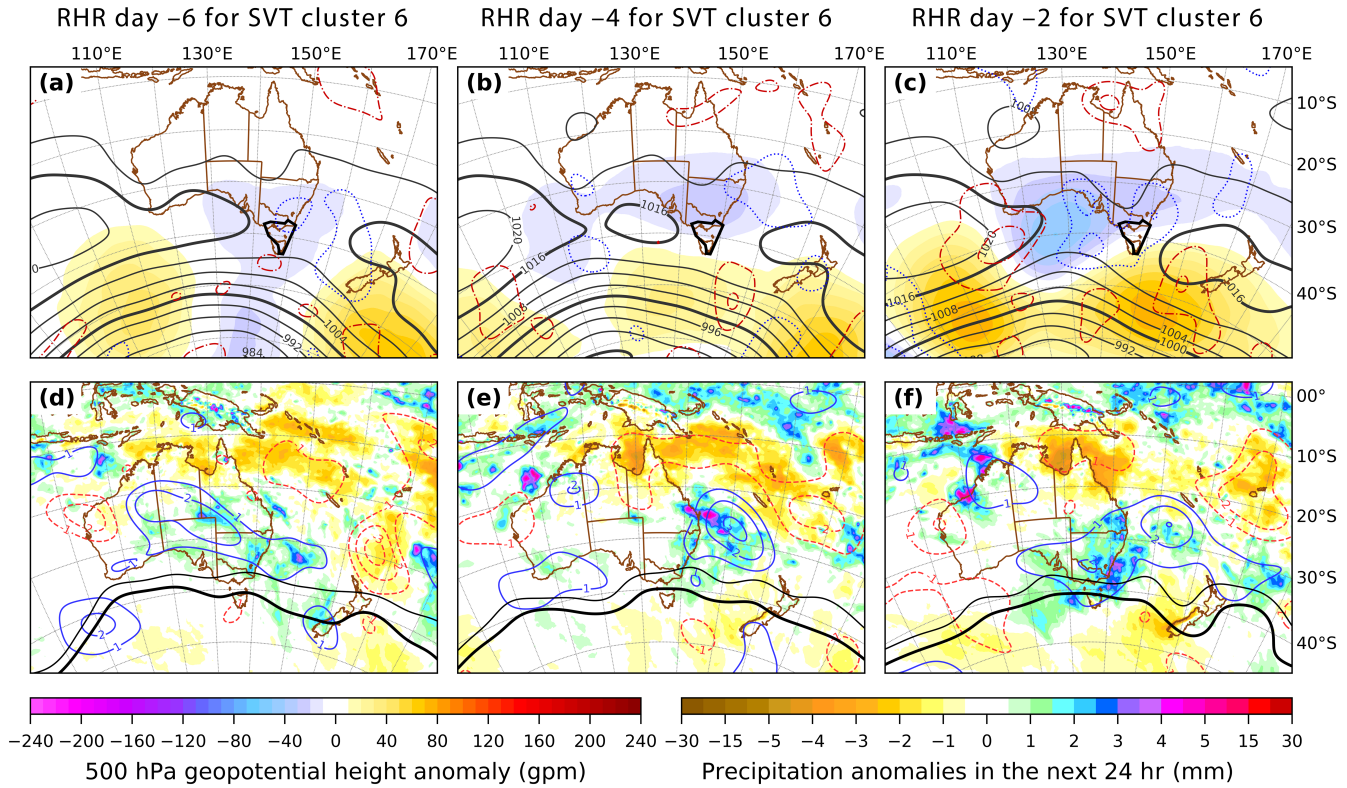

FIGURE 11 As per Figure 6 but for cluster 6, southern Victoria and eastern Tasmania (SVT) subdomain. [Colour figure can be viewed at wileyonlinelibrary.com]

1477870x, 0, Downloaded from https://rmets.onlinelibrary.wiley.com/doi/10.1002/qj.4936 by Karlsruher Institut Für Technologie, Wiley Online Library on [31/03/2025]. See the Terms and Conditions (https://onlinelibrary.wiley.com/terms-and-conditions) on Wiley Online Library for rules of use; OA articles are governed by the applicable Creative Commons License

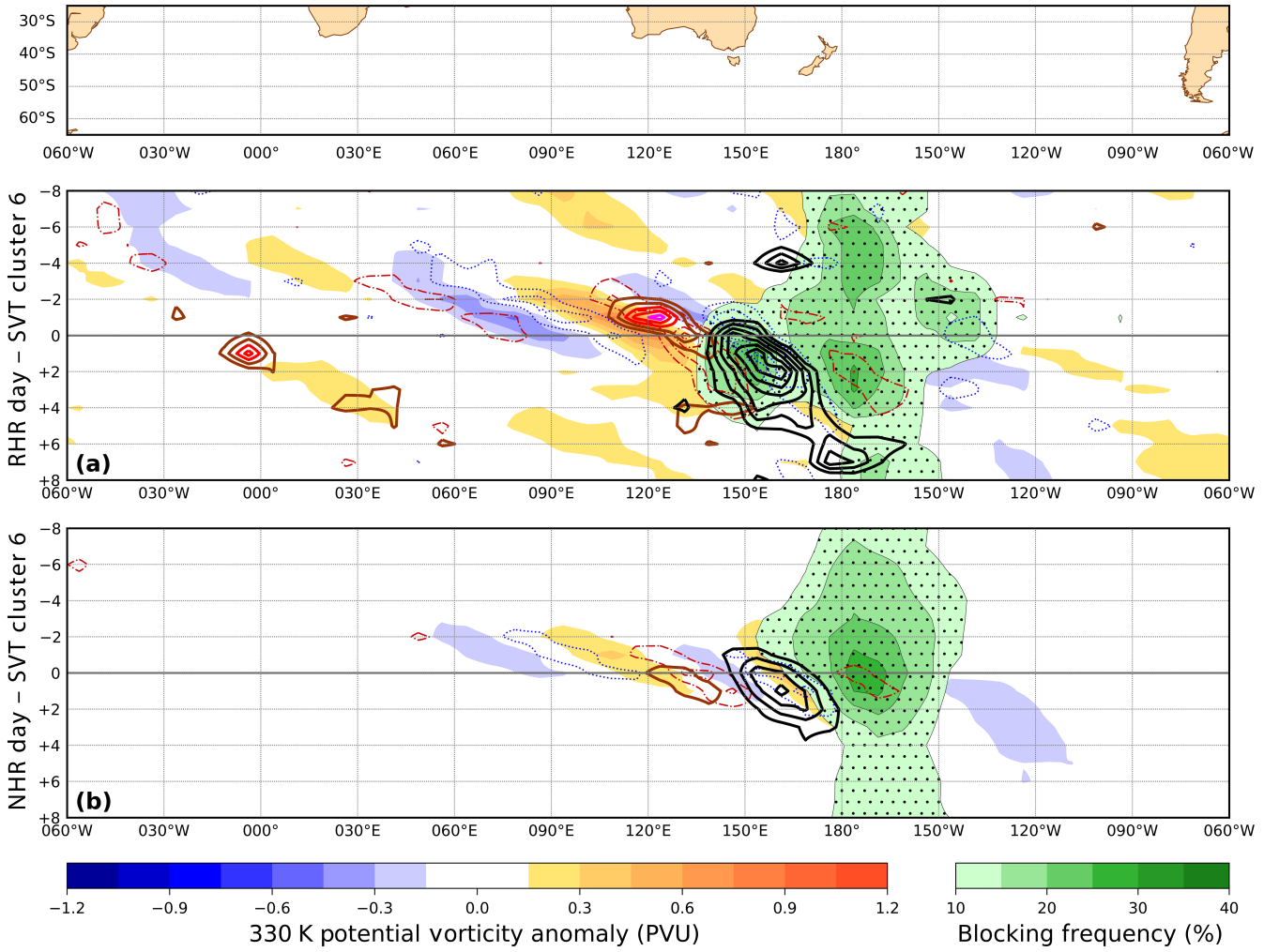

FIGURE 12 As per Figure 7 but for cluster 6, southern Victoria and eastern Tasmania (SVT) subdomain. [Colour figure can be viewed at wileyonlinelibrary.com]

why the signatures of cyclonic Rossby wave breaking in Figures 7 and 12 persist longer than those of anticyclonic Rossby wave breaking. As reported by (Barnes *et al.*, 2024), cyclonic Rossby wave breaking generally occurs after and downstream of anticyclonic Rossby wave breaking.

Cyclonic Rossby wave breaking on RHR days occurs during and after the rainfall and mostly downstream of the region of peak blocking frequency near 155°E. For NHR days, the wave-breaking frequencies are reduced, and their maxima are further east and occur from day 0 onwards. Blocking frequency east of 180° on NHR days is roughly three times the climatological frequency for those longitudes at day 0 but does not appear to be directly related to Rossby wave breaking in cluster 6.

4.4 | Cluster 5, SVT subdomain

The pre-frontal meteorology of cluster 5 is distinct from the cases examined so far, as the 500 hPa geopotential height anomalies remain connected to the midlatitude westerlies on both RHR and NHR days (Figure 13a–c). Greater amplification of the Rossby wave on RHR days is statistically significant and is evident in both the pressure and omega anomaly fields. The vertical motion maximum on RHR days is stronger than the other cases presented and is consistent with a strong cross-frontal circulation. Convection in the Australian Tropics is very active on RHR days, but not on NHR days (Figure 13d–f). A vast plume of moisture extends across the continent into the southwestern Tasman Sea on RHR days and is associated with a pronounced poleward displacement of the dynamic tropopause at 350 K. Precipitable water anomalies are in excess of 15 mm to the northwest of Victoria (Figure 13d–f). The patterns on RHR days are quite similar to the cluster 1 fields of Warren *et al.* (2021, their fig.s 13 and 14). for Melbourne heavy rainfall days.

The PV anomalies and anticyclonic Rossby wave breaking in cluster 5 are shown at 350 K in Figure 14, as the anticyclonic Rossby wave breaking is considerably

1477870x, 0, Downloaded from https://rmets.onlinelibrary.wiley.com/doi/10.1002/qj.4936 by Karlsruher Institut Für Technologie, Wiley Online Library on [31/03/2025]. See the Terms and Conditions (https://onlinelibrary.wiley.com/terms-and-conditions) on Wiley Online Library for rules of use; OA articles are governed by the applicable Creative Commons License

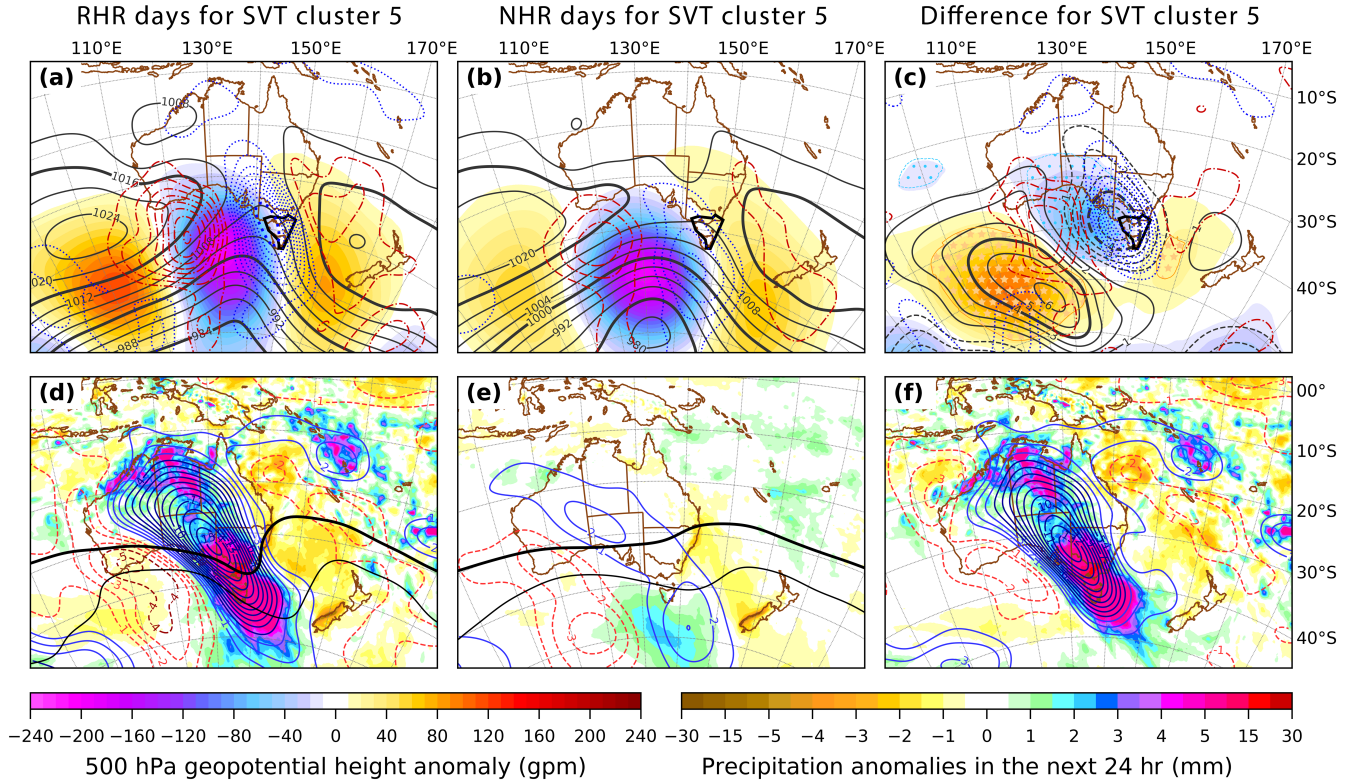

FIGURE 13 As per Figure 5 but for cluster 5, southern Victoria and eastern Tasmania (SVT) subdomain. Here, the solid black contours in (d) and (e) are the −2 PVU (bold) and −4 PVU contours of potential vorticity (PV) at 350 K, rather than at 330 K. [Colour figure can be viewed at wileyonlinelibrary.com]

stronger at this level on RHR days than at 330 K. This is presumably due to the upper tropospheric air associated with the wave breaking being of tropical, rather than midlatitude, origin (e.g., Figure 13d). Anticyclonic Rossby wave breaking is quite common near 90°E 1 day prior to RHR days, but it is greatly enhanced between 160°E and 165°W *following* RHR days. This leads to blocking immediately downstream with a frequency that exceeds 40% near 170°W on day +2. Eastern parts of the North Island of New Zealand experience warmer and wetter summer weather when blocking develops to its east (Kidson, 2000; Renwick, 2011), whereas southwestern parts of the North Island and much of the South Island experience warmer and drier summer weather in this scenario.

The link between heavy precipitation and the subsequent anticyclonic Rossby wave breaking and blocking can be explained by the vertical redistribution of PV that occurs with midtropospheric latent heating. The upper tropospheric anticyclonic PV anomalies that result from this process are known to cause anticyclonic Rossby wave breaking in other circumstances, such as southeast Australian heatwaves, by perturbing the midlatitude waveguide (Archambault *et al.*, 2013; Parker *et al.*, 2013; Quinting & Reeder, 2017). In cluster 5, a poleward displacement of the dynamic tropopause in the vicinity of the heavy rainfall (the −2 PVU contour at 350 K in Figure 13d) is already evident prior to the enhanced anticyclonic Rossby wave breaking that follows the heavy rain (Figure 14a).

In each of clusters 3, 4, and 6, heavy rainfall is associated with a cut-off upper cyclonic anomaly that is *preceded* by anticyclonic Rossby wave breaking at a lead of 1–2 days. However, peak blocking frequencies near 140°E and further east occur *after* RHR days with a lag of 1–2 days (Figures 7, 9, and 12). Although the meteorology of cluster 5 heavy rainfall is different, anticyclonic Rossby wave breaking again precedes the rainfall (near 90°E) and strong blocking follows it. This strongly suggests that the latent heating associated with heavy rainfall is playing an important role in the development of blocking at southeast Australian and New Zealand longitudes during the austral summer.

Anticyclonic Rossby wave breaking is the dynamical process that unifies this study with its counterpart Henderson *et al.* (2024) and is common at the longitudes of southeastern Australia during the austral summer. The amplified, slow-moving upper ridge of these anticyclonic wave breaks coincides with the upper anticyclone in Victorian heatwaves, and positive rainfall anomalies occur in the rising air along the narrow upper trough on its northeastern flank (Parker *et al.*, 2013, 2014). An analysis of

1477870x, 0, Downloaded from https://rmets.onlinelibrary.wiley.com/doi/10.1002/qj.4936 by Karlsruher Institut Für Technologie, Wiley Online Library on [31/03/2025]. See the Terms and Conditions (https://onlinelibrary.wiley.com/terms-and-conditions) on Wiley Online Library for rules of use; OA articles are governed by the applicable Creative Commons License

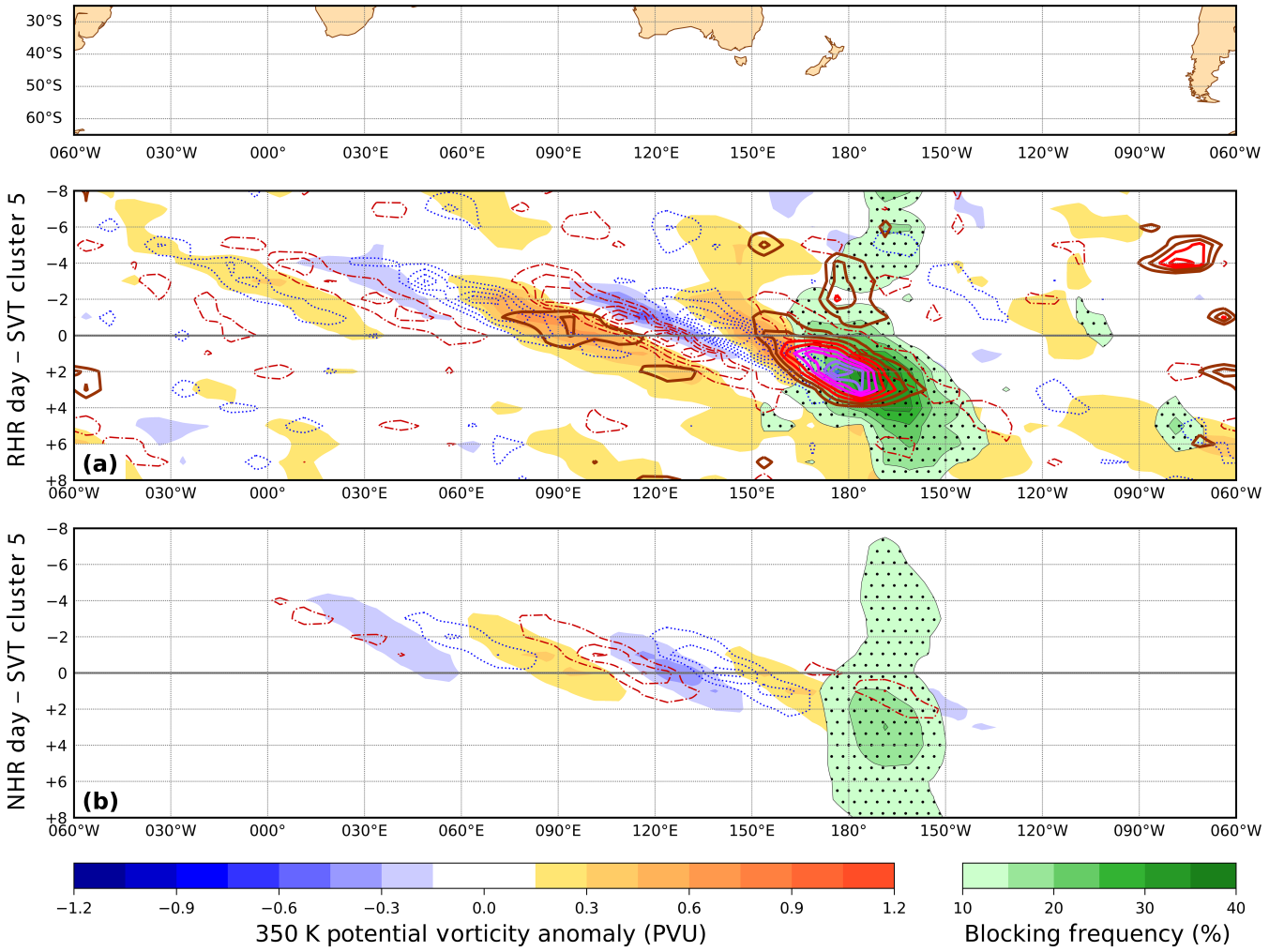

FIGURE 14 As per Figure 7 but for cluster 5, southern Victoria and eastern Tasmania (SVT) subdomain, with the potential vorticity (PV) anomalies and Rossby wave breaking shown at 350 K instead of 330 K. [Colour figure can be viewed at wileyonlinelibrary.com]

equatorward LC1 versus poleward P2 anticyclonic Rossby wave breaking (Peters & Waugh, 1996) has not been undertaken, but Ndarana and Waugh (2011) found that the two types occur with roughly equal frequency at 330 K in the Southern Hemisphere. For Victorian heatwaves, the persistent slow-moving anticyclone is a feature in common with P2 anticyclonic Rossby wave breaking, whereas the filamented upper trough and period of weak anticyclonic anomalies that follow (Henderson *et al.*, 2024; Parker *et al.*, 2014) are consistent with the latter stages of the LC1 baroclinic life cycle (Thorncroft *et al.*, 1993). Heavy rainfall results when the equatorward extremity of the upper trough wraps up cyclonically to form a slow-moving cut-off cyclone (Barnes *et al.*, 2023). Furthermore, the cold fronts that result in heavy rainfall over Victoria and Tasmania tend to be those that form on the western edge of an anticyclonic Rossby wave break (Figures 13 and 14).

Thus, the same dynamical process is responsible for both heatwaves and heavy rainfall in southeastern Australia, and the extent to which a particular location experiences one or the other largely depends on its proximity to the ridges and troughs associated with the PV overturning. For heatwaves and cold frontal heavy rainfall in Victoria, anticyclonic Rossby wave breaking is more frequent at 350 K than at 330 K. As outlined previously, this is presumably because the onset of wave breaking in these cases is closely linked with tropical convection. The tropical tropopause lies close to 350 K, and the subsequent transport of anticyclonic PV towards the midlatitudes at this level has been shown to amplify anticyclonic anomalies in the midlatitude jet stream (Archambault *et al.*, 2013; Parker *et al.*, 2013). In contrast, for heavy rainfall in northeastern NSW, anticyclonic Rossby wave breaking is more usual at 330 K. The cut-off cyclone forms on the leading edge of an equatorward extrusion of cyclonic PV air from the midlatitudes, where the tropopause level is closer to 330 K. Equatorward excursions of cyclonic PV air at 350 K in anticyclonic Rossby wave breaking during heatwaves

1477870x, 0, Downloaded from https://rmets.onlinelibrary.wiley.com/doi/10.1002/qj.4936 by Karlsruher Institut Für Technologie, Wiley Online Library on [31/03/2025]. See the Terms and Conditions (https://onlinelibrary.wiley.com/terms-and-conditions) on Wiley Online Library for rules of use; OA articles are governed by the applicable Creative Commons License

TABLE 3 Number and percentage of wet days, power λ of the symmetry-producing Box–Cox transformation applied to wet-day rainfall, and rainfall amounts (mm) corresponding to 0–3 standard deviation intervals σ above the mean μ of the transformed wet-day rainfall, and the maximum wet-day rainfall, for the cluster and subdomain cases discussed in Sections 4 and 5.

Subdomain	Cluster	Wet days	λ	μ	$\mu+\sigma$	$\mu+2\sigma$	$\mu+3\sigma$	Max
NEC	3	698 (99.7%)	0.1585	3.3	12.5	37.1	88.5	99.3
NEC	4	776 (98.2%)	0.0948	1.8	9.3	30.0	61.5	104.4
SVT	6	778 (98.2%)	0.1172	1.7	7.2	19.1	38.1	46.7
SVT	5	571 (100.0%)	0.0262	0.6	4.2	13.1	20.7	21.7

Abbreviations: NEC, northern coast of eastern New South Wales; SVT, southern Victoria and eastern Tasmania.

may produce less heavy rain on average because baroclinic interactions with near-surface air are hindered by greater vertical separation (Barnes *et al.*, 2021). The strong maximum in blocking frequency east of New Zealand that follows RHR days over the SVT subdomain in cluster 5 (Figure 14a) is consistent with these cases having a high frequency of P2 anticyclonic Rossby wave breaking (Gabriel & Peters, 2008; Peters & Waugh, 1996). However, further investigation of this hypothesis is beyond the scope of this study.

5 | SENSITIVITY OF REGIONALLY AVERAGED RAINFALL

In this section the sensitivity of area-averaged rainfall to selected pressure and moisture anomaly fields is investigated over the two subdomains. Clusters 3 and 4 are analysed separately for the NEC subdomain, and clusters 5 and 6 for the SVT subdomain. In each case, only days where at least one grid point in the subdomain experienced a wet day (≥1 mm) are included.

The ensemble sensitivity technique (see Section 2) is used and consists of a linear regression of the daily rainfall values onto a precursor meteorological anomaly field at each grid point, scaled by the standard deviation of the field. However, daily rainfall distributions are not normally distributed. They usually have pronounced positive skew and are best modelled by a gamma distribution (Martinez-Villalobos & Neelin, 2019). Without accounting for this asymmetry, the results of the linear regressions will be suboptimal; (see Wilks, 2006, Chapter 6.2). Accordingly, the daily wet-day rainfall amounts for each subdomain are re-expressed using the order-preserving and symmetry-producing Box–Cox power transformation T following Wilks (2006, Chapter 3.4). Adopting his notation, for a cluster with $i = 1 \ldots N$ such wet days over the chosen subdomain, the daily rainfall values x_i are transformed as follows:

$$T(x_i) = \begin{cases} \frac{x_i^{\lambda}-1}{\lambda}, & \lambda \neq 0 \\ \ln x_i, & \lambda = 0 \end{cases}.$$

The optimal value for the power λ is obtained to four decimal places by maximising $L(\lambda)$, the log-likelihood function for the normal distribution, with the variance of the rainfall values s^2 divided by N rather than $N-1$.

$$L(\lambda) = -\frac{N}{2}\ln s^2(\lambda) + (\lambda-1)\sum_{i=1}^{N}\ln x_i.$$

The transformed rainfall values are then standardised. The value of λ used for each cluster and subdomain combination is shown in Table 3, along with the area-averaged rainfall values corresponding to the mean and the first, second, and third standard deviations above the mean of the transformed and normalised rainfall distributions. The mean of the transformed rainfall corresponds to the median of the wet-day rainfall.

Thus, the ensemble sensitivity is computed for the transformed and normalised daily area-averaged rainfall. With this adjustment, the results can be interpreted as the linear response in the transformed and normalised rainfall in standard deviations from the transformed mean to a one standard deviation change in the covarying meteorological anomaly field. Hereafter, in this section, the term "transformed rainfall" will refer to the transformed and normalised daily area-averaged wet-day rainfall.

The sensitivity of transformed rainfall to anomalies of 500 hPa geopotential height, MSLP, averaged 400–600 hPa omega, and precipitable water is shown in Figure 15 for day 0 (the composite dates of Figures 5, 8, 10, and 13 respectively), together with a contoured overlay of the cluster-mean anomalies for the aforementioned fields. Regions of positive/negative sensitivity indicate that an increase/decrease in the field value there is associated with an increase in transformed rainfall over the selected subdomain.

1477870x, 0, Downloaded from https://rmets.onlinelibrary.wiley.com/doi/10.1002/qj.4936 by Karlsruher Institut Für Technologie, Wiley Online Library on [31/03/2025]. See the Terms and Conditions (https://onlinelibrary.wiley.com/terms-and-conditions) on Wiley Online Library for rules of use; OA articles are governed by the applicable Creative Commons License

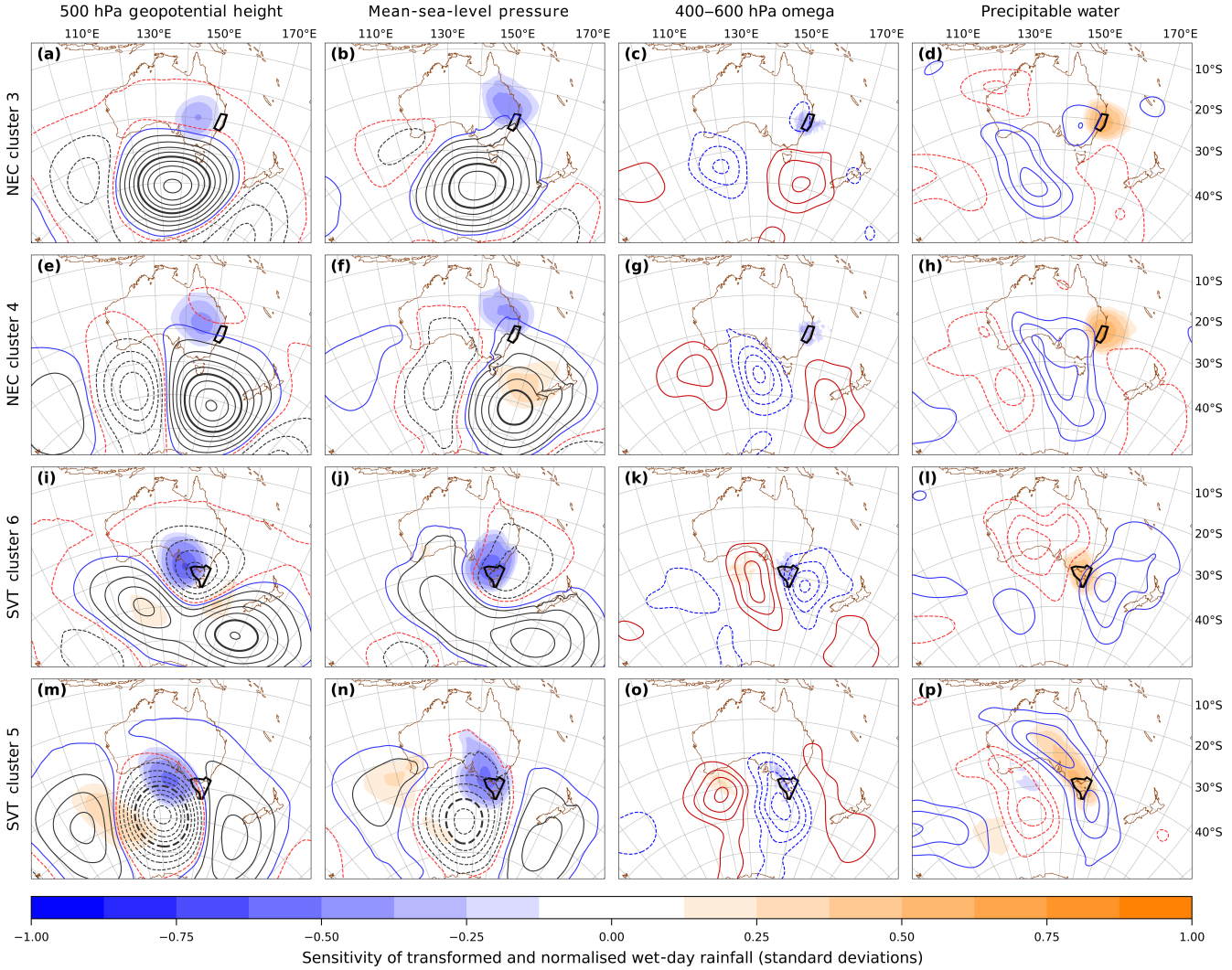

FIGURE 15 Sensitivity of transformed and normalised wet-day rainfall over the next 24 hr (fill) to anomalies of (a, e, i, m) 500 hPa geopotential height, (b, f, j, n) mean-sea-level pressure, (c, g, k, o) 400–600 hPa omega, (d, h, l, p) and precipitable water on day 0. Rainfall is averaged over the area of the illustrated subdomains (black polygons) as follows: northern coast of eastern New South Wales (NEC) in (a–d) cluster 3 and (e–h) cluster 4; and southern Victoria and eastern Tasmania (SVT) in (i–l) cluster 6 and (m–p) cluster 5. Contours (zero omitted) are cluster-mean anomalies: 500 hPa geopotential height, black every 20 gpm with negative dashed, ±100 gpm bold, +5 gpm blue, −5 gpm red; MSLP, black every 2 hPa, negative dashed, ±10 hPa bold, +1 hPa blue, −1 hPa red; averaged 400–600 hPa omega every 0.02 Pa· s^{-1} with blue negative (ascent) and red dashed positive (subsidence); and precipitable water every 1 mm with blue positive and red dashed negative. [Colour figure can be viewed at wileyonlinelibrary.com]

5.1 | NEC subdomain

Transformed rainfall over the NEC subdomain is increased when 500 hPa geopotential height is decreased over southern Queensland and northern NSW (Figure 15a,e) and MSLP is decreased over eastern Queensland and northeastern NSW (Figure 15b,f). There is sensitivity to midtropospheric ascent over the subdomain (Figure 15c,g) but not elsewhere. Ascending motion near the NEC subdomain in the cluster 3 mean (Figure 15c) is largely due to the strong ascent that occurs there on RHR days (compare with Figure 5a,b). The spatial configuration of sensitivity to reduced 500 hPa geopotential height slightly westward of reduced MSLP, and ascending motion east and slightly poleward of the 500 hPa sensitivity, is consistent with increased rainfall in response to the near proximity of a cyclonic baroclinic system. The negative sensitivities in these pressure fields lie on the northern flank of the large anticyclonic anomalies in the cluster means and have an almost identical location to the areas of reduced 500 hPa geopotential height and MSLP associated with RHR days in these clusters (Figures 5a,c and 8a,c).

There is no sensitivity to the anticyclonic pressure anomalies south of mainland Australia in cluster 3. The

1477870x, 0, Downloaded from https://rmets.onlinelibrary.wiley.com/doi/10.1002/qj.4936 by Karlsruher Institut Für Technologie, Wiley Online Library on [31/03/2025]. See the Terms and Conditions (https://onlinelibrary.wiley.com/terms-and-conditions) on Wiley Online Library for rules of use; OA articles are governed by the applicable Creative Commons License

same is true of cluster 4 at 500 hPa. However, transformed rainfall in cluster 4 is increased when the surface pressure is increased to the north of the cluster-mean MSLP anomaly in the south Tasman Sea, and is consistent with the stronger high-pressure system west of New Zealand on RHR days (Figure 8a–c). The couplet of negative/positive sensitivity to MSLP to the north/southeast of the NSW coast implies that transformed rainfall in cluster 4 over the NEC subdomain increases with the strength of the easterly component of the surface wind (Black & Lane, 2015; Rakich *et al.*, 2008). However, the positive sensitivity to MSLP is around 10° east and 30° poleward of the negative sensitivity. Together with the sensitivity to cyclonic development near the NEC subdomain, this points to anticyclonic Rossby wave breaking as the underlying mechanism for this more easterly shift in cluster 4. Figures 7a and 9a show that anticyclonic Rossby wave breaking on the 330 K isentropic surface occurs at three or more times the climatological frequency from 125°E to 150°E on and prior to RHR days.

Transformed rainfall also increases when precipitable water in the vicinity of the NEC subdomain increases (Figure 15d,h). The sensitive regions closely match those of positive precipitable water anomalies >3 mm on RHR days (Figures 5d,f and 8d,f). The sensitivity to precipitable water occurs on the eastern flank of the negative sensitivity to 500 hPa geopotential height, locations that are well to the east of the precipitable water maxima of the cluster means.

The positive precipitable water anomalies about the NEC subdomain on and 2 days prior to RHR days (Figures 5d, 6f, 8d) are broadly consistent with the result of Holgate *et al.* (2020, fig. 3b). They showed that the main moisture source for summer precipitation over the Murray–Darling basin of inland NSW and Queensland is from the region spanning the northern Tasman Sea and southern Coral Sea, west of 160°E. However, the sensitivity of transformed rainfall to precipitable water is very local to the NEC subdomain, even though RHR days also show active convection in the Australian Tropics and elevated moisture over the continent in the 6-day lead-up to RHR days (Figure 6d–f). Anomalies of increased/decreased precipitable water are positively correlated with regions of ascent/subsidence (Figures 5, 6, 8). This result indicates that the transformed rainfall has little sensitivity to moisture outside of regions with large upward vapour transport (Warren *et al.*, 2021). It implies that local flow associated with a nearby cyclonic system is a critical factor in concentrating the large transports of moisture from the east or northeast that occur with heavy precipitation events over the eastern seaboard Barnes *et al.* (2023); White *et al.* (2022); Warren *et al.* (2021). This is not an argument to claim that remote sources of moisture are unimportant. The result may simply mean that the proximity of moisture sources is diverse enough, or that the relationship between column water vapour and heavy rainfall may be sufficiently indirect or nonlinear, to be not well captured by the sensitivity analysis.

5.2 | SVT subdomain

Transformed rainfall over the SVT subdomain in cluster 6 increases with cyclonic baroclinic development that is deeper and slightly westward of that corresponding to the cluster mean (Figure 15i–l). The sensitivity to the pressure field is stronger than with clusters 3 and 4 for the more equatorward NEC subdomain, whereas the sensitivity to precipitable water is weaker. Amplification of the Rossby wave train contributes to increased rainfall as there are positive sensitivities to both the upstream positive geopotential height anomaly at 500 hPa, and the midtropospheric subsidence on its northeastern flank south of the Great Australian Bight. The sensitivity to increased 500 hPa geopotential height in the southern Tasman Sea is consistent with the statistically significant increase in geopotential height there on RHR days (Figure 10c), and its elongated shape has a northnortheast to southsouthwest tilt that is consistent with the cyclonic Rossby wave breaking east of Tasmania that accompanies and follows heavy rainfall days (Figure 12a).

The sensitivity to increased precipitable water and midtropospheric ascent is again highly localised about the SVT subdomain. It occurs on the western flank of the cluster-mean maxima of both fields, which are situated in the southwest Tasman Sea. This sensitivity is coincident with the negative sensitivity to MSLP and on the eastern flank of the sensitive region to reduced 500 hPa geopotential height. The combined sensitivities reinforce the conclusion from Section 4 that the heaviest cluster 6 rainfall over the SVT subdomain occurs when a deeper, more amplified upper cyclonic disturbance develops several degrees westward of its cluster-mean position, which itself follows enhanced anticyclonic Rossby wave breaking near 120°E.

Transformed rainfall over the SVT subdomain in cluster 5 shows greater sensitivity to Rossby wave propagation than all the cases previously examined (Figure 15m–p). It increases when 500 hPa geopotential height and MSLP are reduced on the equatorward flank of their corresponding cluster-mean negative anomalies, and when both pressure fields increase on the eastern flank of the upstream cluster-mean positive anomalies. Together, these indicate that rainfall increases when the wavelength of the approaching Rossby wave shortens and it propagates equatorward of its cluster-mean location east of 120°E.

1477870x, 0, Downloaded from https://rmets.onlinelibrary.wiley.com/doi/10.1002/qj.4936 by Karlsruher Institut Für Technologie, Wiley Online Library on [31/03/2025]. See the Terms and Conditions (https://onlinelibrary.wiley.com/terms-and-conditions) on Wiley Online Library for rules of use; OA articles are governed by the applicable Creative Commons License

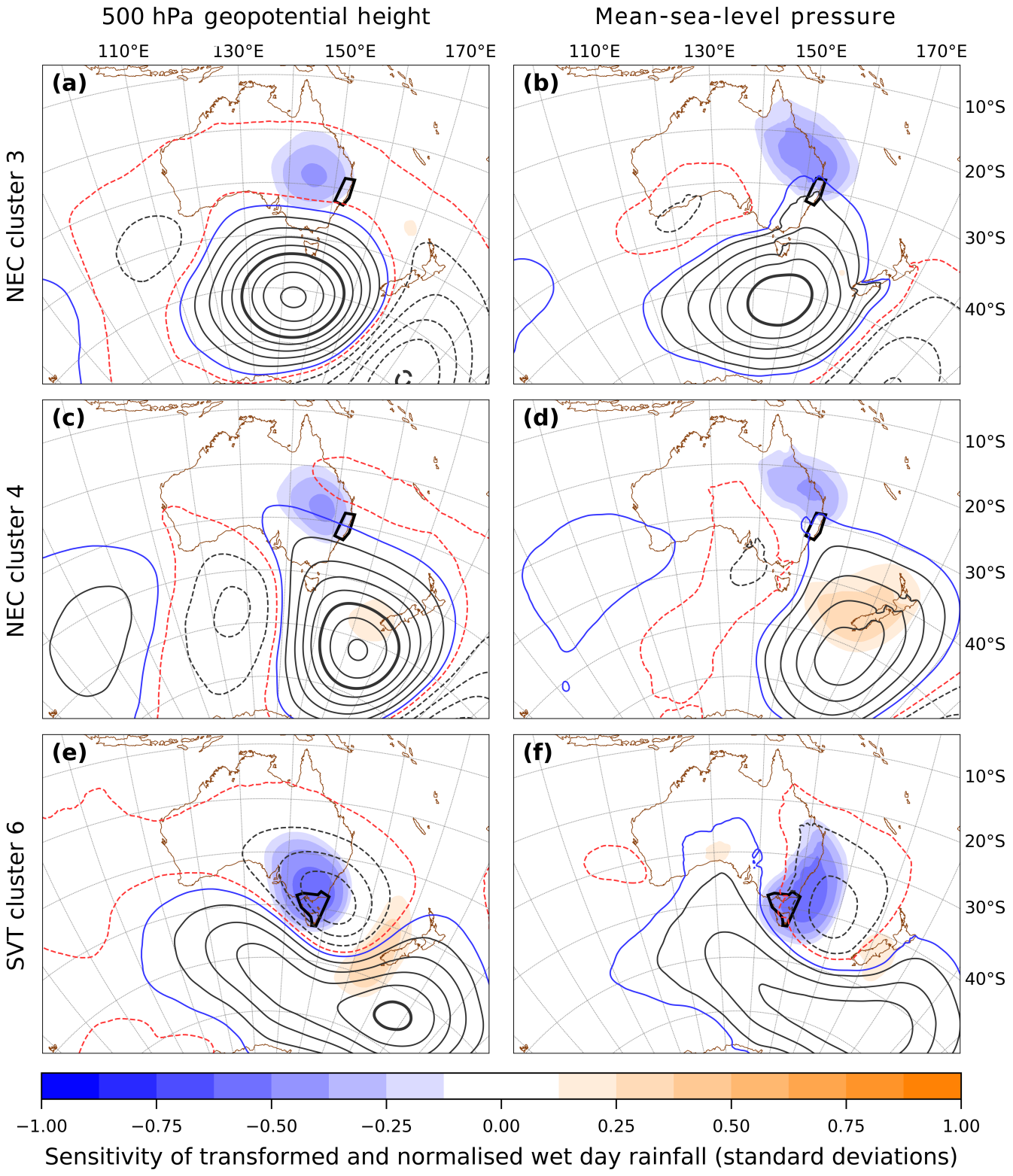

FIGURE 16 As per Figure 15a,b,e,f,i,j, but for day +1, 24 hr after the time of the cluster composites. [Colour figure can be viewed at wileyonlinelibrary.com]

Midtropospheric flow over the SVT subdomain in cluster 5 is northwesterly (see remarks in Section 3). Unlike the other cases, the transformed rainfall is sensitive to moisture upwind, and the sensitive region is co-located with the precipitable water maximum over Australia of the cluster mean. This has a linear shape consistent with a

1477870x, 0, Downloaded from https://rmets.onlinelibrary.wiley.com/doi/10.1002/qj.4936 by Karlsruher Institut Für Technologie, Wiley Online Library on [31/03/2025]. See the Terms and Conditions (https://onlinelibrary.wiley.com/terms-and-conditions) on Wiley Online Library for rules of use; OA articles are governed by the applicable Creative Commons License

moist warm conveyor belt ahead of an approaching cold front (Figure 15p). Transformed rainfall increases with stronger ascent ahead of the front and stronger subsidence behind it (Figure 15o). There is a strong spatial correlation between the vertical motion and precipitable water fields with moist/dry air occurring slightly to the east of regions with ascending/subsiding midtropospheric air. This explains the sensitivity to moisture in the upstream Rossby wave. These sensitivities are found progressively farther to the east of the cluster-mean moisture extrema as one travels upstream from the SVT subdomain, again consistent with an increase in transformed rainfall as wavelength shortens. Overall, these results support the finding of Section 4 that heavy rainfall in this cluster occurs with a more amplified front that draws greater moisture ahead of it from the Australian Tropics.

The sensitivity of transformed rainfall to the precursor meteorological fields in Figure 15 was also tested at several lead times (not shown). Similar results are obtained for day −1 but are weaker than day 0. The negative day −1 sensitivity to 500 hPa geopotential height and MSLP is shifted west by around 10° for cluster 6 and cluster 5, south and west by 5° for cluster 3, and west by 3° for cluster 4. The latter two signatures are consistent with cut-off upper cyclonic anomalies that are slow-moving (Barnes *et al.*, 2023). Almost no sensitivity is evident at day −2.

When the sensitivities to the pressure fields are computed forward in time for day +1 (Figure 16), small correlations emerge with increased 500 hPa geopotential height in the eastern Tasman Sea for clusters 3 and 6 and enlarge in the case of cluster 4. A small region of sensitivity to increased MSLP occurs near 43°S, 163°E in cluster 3 and over the south island of New Zealand for cluster 6. The sensitivity to high surface pressure in cluster 4 is larger and shifted east by several degrees. Thus, the sensitivity to high pressure in the Tasman Sea is larger at day +1. Correlations with reduced 500 hPa geopotential height and MSLP near the location of the cut-off upper cyclonic anomaly in each cluster on RHR days are stronger though.

In all of the clusters examined, the transformed subdomain rainfall is sensitive to baroclinic development associated with an upper level cyclonic anomaly to the west of the domain. However, the sensitivity to high pressure is weak and, in all cases but one, emerges only *after* the composite rain has fallen. Pook *et al.* (2013) found that spatial correlations between southeast Australian rainfall and blocking near 140°E are usually highest to the west of that longitude. On that basis, they proposed that the formation of cut-off lows to the north of the anticyclone in blocking events is the main reason for the correlation. The DJFM results presented here strongly support that hypothesis and provide additional evidence from a temporal perspective.

6 | CONCLUSIONS

Heavy rainfall days during an extended DJFM austral summer have been studied over two heavily populated regions of southeastern Australia. The importance of several known meteorological ingredients of heavy rainfall have been assessed by comparing their spatial distributions with those of NHR days that have a similar synoptic-scale 500 hPa geopotential height pattern. A synoptic climatology of seven weather states was constructed by *k*-means cluster analysis of daily ERA5 500 hPa geopotential height anomalies at 0000 UTC from 40 DJFM austral summers over a domain centred on southeastern Australia. Two of the cluster means are distinctly wetter than the others over large expanses of southeastern Australia. In cluster 3, a positive rainfall anomaly covers most of NSW and southern Queensland, with the largest anomalies over the northeastern coast of NSW. The mean state of cluster 6 has positive rainfall anomalies over Victoria, Tasmania, and southeastern NSW.

Subdomains were chosen over NEC and over SVT to study heavy rainfall in these wettest clusters. The 0.05° × 0.05°gridded AWAP dataset was used and RHR days over each subdomain were defined as any day on which 5% or more of the land area received grid-point wet-day rainfall above their 95th DJFM percentile. All DJFM days that did not meet this threshold in the subdomain were termed NHR days. The synoptic-scale differences between RHR and NHR days were compared for those clusters in which heavy rainfall days occur most often. A symmetry-producing transformation was then applied to area-averaged wet-day rainfall over these subdomains to study the spatial sensitivity of rainfall to several relevant meteorological fields.

Clusters 3 and 4 have the greatest number of RHR days for the NEC subdomain. These cluster means have surface high-pressure centres south of mainland Australia and in the Tasman Sea respectively, and they flow with an easterly component onto the NSW coast. Both heavy rainfall composites show a cut-off upper cyclonic anomaly to the west of the NEC subdomain that is either not present or dramatically weaker on NHR days. Though the mean surface flow on NHR days is southeasterly, reduced MSLP on the eastern flank of a cut-off upper cyclonic anomaly results in a stronger surface flow that is easterly on RHR days. Strong midtropospheric ascent occurs over the NEC subdomain on RHR days that is absent on NHR days, and the spatial configuration of the upper and lower tropospheric pressure anomalies in relation to the midtropospheric ascent is consistent with cyclonic baroclinic development. As RHR days in cluster 4 are often preceded by RHR days in cluster 3, with only minor differences in the location of the cut-off upper cyclonic anomaly, these results support the

1477870x, 0, Downloaded from https://rmets.onlinelibrary.wiley.com/doi/10.1002/qj.4936 by Karlsruher Institut Für Technologie, Wiley Online Library on [31/03/2025]. See the Terms and Conditions (https://onlinelibrary.wiley.com/terms-and-conditions) on Wiley Online Library for rules of use; OA articles are governed by the applicable Creative Commons License

finding of Barnes *et al.* (2023) that the key driving ingredient of heavy summer precipitation along the eastern seaboard is a slow-moving cut-off upper cyclonic anomaly. This cut-off upper cyclonic anomaly is a feature of the anticyclonic Rossby wave breaking that occurs in the 2 days leading up to the heavy rain.

Positive precipitable water anomalies on RHR days are largely coincident with the ascending motion anomalies centred on the NEC subdomain. The sensitivity of rainfall to precipitable water in clusters 3 and 4 is local, almost radially symmetric about the NEC subdomain, strongly correlated with vigorous ascending motion, and well removed from precipitable water maxima in the cluster mean. This suggests that heavy rainfall is mostly sensitive to upward vapour transport, the location of which is largely determined by the wind field induced by cyclonic baroclinic development.

The results for cluster 6 rainfall over the SVT subdomain are similar, although the upper cyclonic anomaly is not as clearly cut off as it is with clusters 3 and 4. An upper trough is a mean characteristic of cluster 6 but is more amplified and situated further west when heavy rainfall occurs over the SVT subdomain, where it is again preceded by anticyclonic Rossby wave breaking. SVT rainfall has higher sensitivity to pressure and lower sensitivity to moisture than its NEC counterparts, presumably reflecting its higher latitude. The sensitivity to moisture is again local to the subdomain and coincident with the ascending motion anomaly downstream of the upper trough.

Heavy rainfall in cluster 5 is associated with a more amplified Rossby wave that sources moisture from tropical convection over north and northwestern Australia, rather than a local cyclonic baroclinic system. This is the only case examined that shows non-local sensitivity to precipitable water. Rainfall over the SVT subdomain is heavier when the transport of water vapour from the tropical source region is increased. The downstream result of the heavier rainfall is anticyclonic Rossby wave breaking and increased blocking east of New Zealand.

Previous studies have identified blocking as a major driver of rainfall in Australia, although less so over summer. However, the increase in blocking frequency from 135°E to 180° associated with RHR days in clusters 3, 4, and 6 generally *follows* the onset of heavy rain. Blocking anticyclones often occur as a consequence of Rossby wave breaking. Yet, cut-off lows that frequently occur on the equatorward flank of blocking anticyclones are also an outcome of anticyclonic Rossby wave breaking (Ndarana & Waugh, 2010), which is found to occur in the lead-up to heavy rainfall in all three of these clusters. The present study has shown that summer rainfall over southeastern Australia exhibits a strong sensitivity to upper level cyclonic pressure anomalies, but there is no sensitivity to high-pressure anomalies *prior* to the rainfall, except in cluster 4. The results also suggest that latent heat release associated with heavy rainfall may be important in the subsequent development of blocking, especially those of cluster 5. Using the same clusters, the companion study to this article Henderson *et al.* (2024) discussed the prevalence of upper tropospheric anticyclonic Rossby wave breaking in the occurrence of heatwaves south of 30°S over southeastern Australia. Here, this same dynamical process is also found to be responsible for heavy rainfall in the region. Thus, it seems more appropriate to emphasise the upper level cyclones that arise from anticyclonic Rossby wave breaking as the key ingredient of heavy summer rainfall over southeastern Australia, rather than blocking high-pressure systems.

ACKNOWLEDGEMENTS

We gratefully acknowledge funding provided by the Australian Research Council Centre of Excellence for Climate Extremes (CE170100023) and the Australian Research Council Centre of Excellence for the Weather of the 21st Century (CE230100012) for this research. We also acknowledge the National Computing Infrastructure, the European Centre for Medium-range Weather Forecasts for the availability of ERA5, and the Bureau of Meteorology for the AWAP dataset. CRH would like to thank the Bureau of Meteorology Training Centre for time provided to conduct this research, and JFQ the Karlsruhe Institute of Technology. JFQ's contribution was partly funded by the Helmholtz Association as part of the Young Investigator Group "Sub-seasonal Predictability: Understanding the Role of Diabatic Outflow" (SPREADOUT, grant VH-NG-1243). CRH is also grateful to Dr Teresa Parker for her guided introduction to ensemble sensitivity in a previous collaboration. Finally, we would like to thank three anonymous reviewers. Their very thoughtful comments and suggestions greatly improved the manuscript. Open access publishing facilitated by Monash University, as part of the Wiley - Monash University agreement via the Council of Australian University Librarians.

FUNDING INFORMATION

This work was supported by the Australian Research Council, Centre of Excellence for Climate Extremes (grant/award number: CE170100023), the Helmholtz Association, and the Young Investigator Group (SPREADOUT) (grant/award number: VH-NG-1243).

DATA AVAILABILITY STATEMENT

Gridded datasets from the Australian Water Availability Project and ERA5 are available from the Australian National Computing Infrastructure (NCI Australia).

1477870x, 0, Downloaded from https://rmets.onlinelibrary.wiley.com/doi/10.1002/qj.4936 by Karlsruher Institut Für Technologie, Wiley Online Library on [31/03/2025]. See the Terms and Conditions (https://onlinelibrary.wiley.com/terms-and-conditions) on Wiley Online Library for rules of use; OA articles are governed by the applicable Creative Commons License

Derived data supporting the findings of this study are available from the corresponding author CRH on request, including the latitude and longitude arrays that define each subdomain boundary used in this article.

The data that support the findings of this study are available from the corresponding author upon reasonable request.

ENDNOTES

[1]Some researchers define this as the region between 25°S and 35°S east of the Great Dividing Range, e.g. Black and Lane (2015).

[2]Heavy rainfall was defined as those events recording precipitation above the 95th percentile of wet days (≥1 mm) and extreme rainfall as those with precipitation above the 99th percentile of wet days.

ORCID

Cameron R. Henderson https://orcid.org/0009-0001-3109-6100
Michael A. Barnes https://orcid.org/0000-0001-8056-8875
Julian F. Quinting https://orcid.org/0000-0002-8409-2541

REFERENCES

Archambault, H.M., Bosart, L.F., Keyser, D. & Cordeira, J.M. (2013) A climatological analysis of the extratropical flow response to recurving Western North Pacific tropical cyclones. *Monthly Weather Review*, 141, 2325–2346.

Barnes, M.A., King, M.J., Reeder, M.J. & Jakob, C. (2023) The dynamics of slow-moving coherent cyclonic potential vorticity anomalies and their links to heavy rainfall over the eastern seaboard of Australia. *Quarterly Journal of the Royal Meteorological Society*, 149, 2233–2251.

Barnes, M.A., Ndarana, T. & Landman, W.A. (2021) Cut-off lows in the southern hemisphere and their extension to the surface. *Climate Dynamics*, 56, 3709–3732.

Barnes, M.A., Reeder, M.J. & Ndarana, T. (2024) Rossby wave breaking morphologies on the southern hemisphere dynamical tropopause. *Journal of Climate*.

Berrisford, P., Hoskins, B.J. & Tyrlis, E. (2007) Blocking and Rossby wave breaking on the dynamical tropopause in the southern hemisphere. *Journal of the Atmospheric Sciences*, 64, 2881–2898.

Berry, G.J., Reeder, M.J. & Jakob, C. (2012) Coherent synoptic disturbances in the Australia monsoon. *Journal of Climate*, 25, 8409–8421.

Black, M.T. & Lane, T.P. (2015) An improved diagnostic for summertime rainfall along the eastern seaboard of Australia. *International Journal of Climatology*, 35, 4480–4492.

Bureau of Meteorology. (2012) *Exceptional heavy rainfall across southeast Australia*. Tech. Rep. 39. Darlinghurst, NSW: Bureau of Meteorology, p. 19.

Bureau of Meteorology. (2013) *Extreme rainfall and flooding in coastal Queensland and New South Wales*. Tech. Rep. 44. Melbourne, Victoria: Bureau of Meteorology, p. 14.

Bureau of Meteorology. (2016) *Extreme rainfall in northern and eastern Tasmania*. Tech. Rep. 54. Melbourne, Victoria: Bureau of Meteorology, p. 16.

Bureau of Meteorology. (2021) *Extreme rainfall and flooding in eastern and central Australia in March 2021*. Tech. Rep. 74. Melbourne, Victoria: Bureau of Meteorology, p. 21.

Bureau of Meteorology. (2022) *Extreme rainfall and flooding in south-eastern Queensland and eastern New South Wales*. Tech. Rep. 76. Melbourne, Victoria: Bureau of Meteorology, p. 29.

Bureau of Meteorology. (2024) Average annual, seasonal and monthly rainfall maps. http://www.bom.gov.au/climate/maps/averages/rainfall/

Callaghan, J. & Power, S.B. (2014) Major coastal flooding in south-eastern Australia 1860-2012, associated deaths and weather systems. *Australian Meteorological and Oceanographic Journal*, 64, 183–213.

Coughlan, M.J. (1983) A comparative climatology of blocking action in the two hemispheres. *Australian Meteorological Magazine*, 31, 3–13.

de Vries, A.J. (2021) A global climatological perspective on the importance of rossby wave breaking and intense moisture transport for extreme precipitation events. *Weather and Climate Dynamics*, 2, 129–161.

Gabriel, A. & Peters, D. (2008) A diagnostic study of different types of Rossby wave breaking events in the northern Extratropics. *Journal of the Meteorological Society of Japan*, 86, 613–631.

Gimeno, L., Drumond, A., Nieto, R., Trigo, R.M. & Stohl, A. (2010) On the origin of continental precipitation. *Geophysical Research Letters*, 37(1), 7.

Henderson, C.R., Reeder, M.J., Parker, T.J., Quinting, J.F. & Jakob, C. (2024) Summer heatwaves in Southeastern Australia. *Quarterly Journal of the Royal Meteorological Society*, 150(764), 4285–4305.

Hersbach, H., Bell, B., Berrisford, P., Hirahara, S., Horányi, A., Sabater, J.M. et al. (2020) The ERA5 global reanalysis. *Quarterly Journal of the Royal Meteorological Society*, 146, 1999–2049.

Holgate, C.M., Evans, J.P., van Dijk, A.I.J.M., Pitman, A.J. & Di Virgilio, G. (2020) Australian precipitation recycling and evaporative source regions. *Journal of Climate*, 33, 8721–8735.

Hoskins, B. & Berrisford, P. (1988) A potential vorticity perspective of the storm of 15-16 October 1987. *Weather*, 43, 122–129.

Hoskins, B.J., McIntyre, M.E. & Robertson, A.W. (1985) On the use and significant of isentropic potential vorticity maps. *Quarterly Journal of the Royal Meteorological Society*, 111, 877–946.

Jones, D.A., Wang, W. & Fawcett, R. (2009) High-quality spatial climate data-sets for Australia. *Australian Meteorological and Oceanographic Journal*, 58, 233–248.

Kidson, J.W. (2000) An analysis of New Zealand synoptic types and their use in defining weather regimes. *International Journal of Climatology*, 20, 299–316.

Martinez-Villalobos, C. & Neelin, J.D. (2019) Why do precipitation intensities tend to follow gamma distributions? *Journal of the Atmospheric Sciences*, 76, 3611–3631.

Masato, G., Hoskins, B.J. & Woollings, T.J. (2012) Wave-breaking characteristics of midlatitude blocking. *Quarterly Journal of the Royal Meteorological Society*, 138, 1285–1296.

Narsey, S., Reeder, M.J., Ackerley, D. & Jakob, C. (2017) A Midlatitude influence on Australian monsoon bursts. *Journal of Climate*, 30, 5377–5393.

Ndarana, T. & Waugh, D.W. (2010) The link between cut-off lows and Rossby wave breaking in the southern hemisphere. *Quarterly Journal of the Royal Meteorological Society*, 136, 869–885.

1477870x, 0, Downloaded from https://rmets.onlinelibrary.wiley.com/doi/10.1002/qj.4936 by Karlsruher Institut Für Technologie, Wiley Online Library on [31/03/2025]. See the Terms and Conditions (https://onlinelibrary.wiley.com/terms-and-conditions) on Wiley Online Library for rules of use; OA articles are governed by the applicable Creative Commons License

Ndarana, T. & Waugh, D.W. (2011) A climatology of Rossby wave breaking on the southern hemisphere tropopause. *Journal of the Atmospheric Sciences*, 68, 798–811.

O'Brien, L. & Reeder, M.J. (2017) Southern hemisphere summertime Rossby waves and weather in the Australian region. *Quarterly Journal of the Royal Meteorological Society*, 143, 2374–2388.

Parker, T.J., Berry, G.J. & Reeder, M.J. (2013) The influence of tropical cyclones on heat waves in Southeastern Australia. *Geophysical Research Letters*, 40, 6264–6270.

Parker, T.J., Berry, G.J. & Reeder, M.J. (2014) The structure and evolution of heat waves in Southeastern Australia. *Journal of Climate*, 27, 5768–5785.

Pelly, J.L. & Hoskins, B.J. (2003) A new perspective on blocking. *Journal of the Atmospheric Sciences*, 60, 743–755.

Pepler, A.S., Coutts-Smith, A. & Timbal, B. (2014) The role of East Coast lows on rainfall patterns and inter-annual variability across the East Coast of Australia. *International Journal of Climatology*, 34, 1011–10212.

Pepler, A.S. & Dowdy, A. (2021) Intense east coast lows and associated rainfall in eastern Australia. *Journal of Southern Hemisphere Earth Systems Science*, 71, 110–122.

Peters, D. & Waugh, D.W. (1996) Influence of Barotropic shear on the poleward advection of upper-tropospheric air. *Journal of the Atmospheric Sciences*, 53, 3013–3031.

Pook, M.J., McIntosh, P.C. & Meyers, G.G. (2006) The synoptic decomposition of cool-season rainfall in the Southeastern Australian cropping region. *Journal of Applied Meteorology and Climatology*, 45, 1156–1170.

Pook, M.J., Risbey, J.S., McIntosh, P.C., Ummenhofer, C.C., Marshall, A.G. & Meyers, G.G. (2013) The seasonal cycle of blocking and associated physical mechanisms in the Australian region and relationship with rainfall. *Monthly Weather Review*, 141, 4534–4553.

Quinting, J.F. & Reeder, M.J. (2017) Southeastern Australian heat waves from a trajectory viewpoint. *Monthly Weather Review*, 145, 4109–4125.

Rakich, C.S., Holbrook, N.J. & Timbal, B. (2008) A pressure gradient metric capturing planetary-scale influences on eastern Australian rainfall. *Geophysical Research Letters*, 35, 1–6.

Reeder, M.J., Spengler, T. & Musgrave, R. (2015) Rossby waves, extreme fronts, and wildfires in southeastern Australia. *Geophysical Research Letters*, 42, 2015–2023.

Reid, K.J., O'Brien, T.A., King, A.D. & Lane, T.P. (2021) Extreme water vapor transport during the march 2021 Sydney floods in the context of climate projections. *Geophysical Research Letters*, 48, 1–8.

Renwick, J.A. (2011) Kidson's synoptic weather types and surface climate variability over New Zealand. *Weather and Climate*, 31, 3–23.

Risbey, J.S., Pook, M.J., McIntosh, P.C., Ummenhofer, C.C. & Meyers, G.G. (2009a) Characteristics and variability of synoptic features associated with cool season rainfall in southeastern Australia. *International Journal of Climatology*, 29, 1595–1613.

Risbey, J.S., Pook, M.J., McIntosh, P.C., Wheeler, M.C. & Hendon, H.H. (2009b) On the remote drivers of rainfall variability in Australia. *Monthly Weather Review*, 137, 3233–3253.

Rossow, W.B., Tselioudis, G., Polak, A. & Jakob, C. (2005) Tropical climate described as a distribution of weather states indicated by distinct mesoscale cloud property mixtures. *Geophysical Research Letters*, 32, 1–4.

Schalge, B., Blender, R. & Fraedrich, K. (2011) Blocking detection based on synoptic filters. *Advances in Meteorology*, 2011, 717812.

Song, J., Li, C., Pan, J. & Zhou, W. (2011) Climatology of anticyclonic and cyclonic Rossby wave breaking on the dynamical tropopause in the southern hemisphere. *Journal of Climate*, 24, 1239–1251.

Speer, M.S., Leslie, L.M. & Fierro, A.O. (2011) Australian east coast rainfall decline related to large scale climate drivers. *Climate Dynamics*, 36, 1419–1429.

Thorncroft, C.D., Hoskins, B.J. & McIntyre, M.E. (1993) Two paradigms of baroclinic-wave life-cycle behaviour. *Quarterly Journal of the Royal Meteorological Society*, 119, 17–55.

Tibaldi, S., Tosi, E., Navarra, A. & Pedulli, L. (1994) Northern and southern hemisphere seasonal variability of blocking frequency and predictability. *Monthly Weather Review*, 122, 1971–2003.

Torn, R.D. & Hakim, G.J. (2008) Ensemble-based sensitivity Analyis. *Monthly Weather Review*, 136, 663–677.

Trenberth, K.E. (1985) Persistence of daily Geopotential Heights over the southern hemisphere. *Monthly Weather Review*, 113, 38–53.

Warren, R.A., Jakob, C., Hitchcock, S.M. & White, B.A. (2021) Heavy versus extreme rainfall events in southeast Australia. *Quarterly Journal of the Royal Meteorological Society*, 147, 3201–3226.

White, B.A., Jakob, C. & Reeder, M.J. (2022) Fundamental ingredients of Australian rainfall extremes. *Journal of Geophysical Research: Atmospheres*, 127, 1–20.

Wilks, D.S. (2006) *Statistical methods in the atmospheric sciences*. International Geophysics Series, Vol. 91, 2nd edition. Burlington, MA, USA: Academic Press.

How to cite this article: Henderson, C.R., Barnes, M.A., Reeder, M.J., Quinting, J.F. & Jakob, C. (2025) Heavy summer rainfall in southeastern Australia. *Quarterly Journal of the Royal Meteorological Society*, e4936. Available from: https://doi.org/10.1002/qj.4936

APPENDIX A. CLUSTER PERSISTENCE AND TRANSITIONS

A flow chart showing the frequency of cluster persistence and transitions at a lag of 1 day is shown in Figure A1. Clusters 1–5 have centroids that resemble amplified phases of Rossby wave propagation. These are arranged in the central row in an order that reflects their usual eastward propagation (relative to Earth's surface). However, it is exceedingly rare for a complete cycle from cluster 1 (a post-frontal regime in Victoria) back to cluster 1 to pass through each of these amplified phases in that order. Normally, a transition to one of the less-amplified meridional dipole clusters 6 or 7 occurs at some point in the cycle, and there is often some back-and-forth between other clusters along the way. Cluster 7 is visited more frequently when the flow is mobile, and cluster 6 occurs more often when large anticyclones form south of eastern Australia or in the Tasman Sea.

1477870x, 0, Downloaded from https://rmets.onlinelibrary.wiley.com/doi/10.1002/qj.4936 by Karlsruher Institut Für Technologie, Wiley Online Library on [31/03/2025]. See the Terms and Conditions (https://onlinelibrary.wiley.com/terms-and-conditions) on Wiley Online Library for rules of use; OA articles are governed by the applicable Creative Commons License

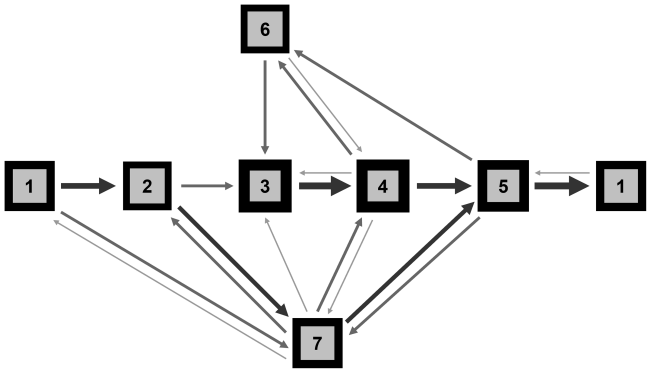

FIGURE A1 Flow chart showing frequency of cluster persistence and transitions at a lag of 1 day. All scenarios that occur ≥1% of the time are shown, accounting for 91% of all cases. Border/arrow thicknesses show the frequency of persistence/transition to the nearest 1%. Arrow thicknesses vary from 1% to 5% of cases and borders 5% to 8% (e.g., persistence of clusters 3 and 4 each represent 8% of all December–March cases).

The number of days on which persistence of a cluster, or a transition between two clusters, occurred over the 40-year period studied is shown in Table A1. For each cluster, day-to-day persistence is more common than a transition with any other single cluster. For instance, from one day to the next, cluster 4 was the destination cluster on 782 occasions. The initial cluster was also cluster 4 on 369 occasions, implying that persistence occurs 47% of the time in cluster 4 at a lag of 1 day. The next most common scenario is a transition from cluster 3. Out of the 413 day-to-day transitions into cluster 4, this occurred 223 times, amounting to 54% of all transitions at a lag of 1 day.

A sequence of cluster transitions is quite well defined at a lag of 1 day but becomes less obvious at longer lags. Over periods of 5 days the number of days in each initial/destination category is almost uniformly distributed (not shown).

TABLE A1 Destination cluster at a lag of 1 day for the initial cluster specified, showing the number of day-to-day periods with cluster persistence (diagonal entries, bold) and cluster transitions (off-diagonal entries)

Destination cluster	1	2	3	4	5	6	7
Cluster 1 initially	**292**	185	4	1	54	28	75
Cluster 2 initially	35	**250**	92	18	24	18	138
Cluster 3 initially	0	18	**384**	223	6	34	30
Cluster 4 initially	5	1	54	**369**	177	116	62
Cluster 5 initially	225	11	2	22	**327**	82	115
Cluster 6 initially	34	43	100	54	35	**260**	45
Cluster 7 initially	49	73	58	95	162	30	**295**
Total							**4810**

1477870x, 0, Downloaded from https://rmets.onlinelibrary.wiley.com/doi/10.1002/qj.4936 by Karlsruher Institut Für Technologie, Wiley Online Library on [31/03/2025]. See the Terms and Conditions (https://onlinelibrary.wiley.com/terms-and-conditions) on Wiley Online Library for rules of use; OA articles are governed by the applicable Creative Commons License